Supplementary Information

Structural Basis of Cycloaddition in Biosynthesis of Iboga and Aspidosperma Alkaloids

Lorenzo Caputi[1#], Jakob Franke[2#], Kate Bussey[3], Scott C. Farrow[3], Ivo Jose Curcino Vieira[4], Clare E. M. Stevenson[3], David M. Lawson*[3], Sarah E. O'Connor*[1]

[1] Max Planck Institute of Chemical Ecology, Department of Natural Product Biosynthesis, Hans-Knöll-Straße 8, 07745 Jena, Germany

[2] Leibniz University Hannover, Centre for Biomolecular Drug Research, Schneiderberg 38, 30167 Hannover, Germany

[3] John Innes Centre, Department of Biological Chemistry, Norwich Research Park, Norwich, NR4 7UH, UK

[4] Laboratorio de Ciencias Quimicas-UENF-Campos dos Goytacazes-RJ, 28013-602, Brazil

[#] These authors contributed equally.

*Correspondence to: oconnor@ice.mpg.de and david.lawson@jic.ac.uk

Supplementary Tables

Supplementary Table 1. X-ray data collection and refinement statistics

	CS	TS	CorS
Data collection			
Space group	$P2_1$	$P2_1$	$P6_522$
Cell dimensions			
a, *b*, *c* (Å)	81.54, 121.03, 157.98	56.49, 108.96, 63.24	82.84, 82.84, 247.56
α, β, γ (°)	90.00, 99.02, 90.00	90.00, 108.54, 90.00	90.00, 90.00, 120.00
Resolution (Å)	52.01 – 2.19 (2.23 – 2.19)	59.95 – 1.30 (1.32 – 1.30)	71.74 – 1.42 (1.44 – 1.42)
R_{merge}	0.093 (1.129)	0.111 (1.680)	0.140 (1.760)
$I / \sigma I$	14.1 (2.0)	10.8 (1.3)	10.4 (2.3)
Completeness (%)	98.3 (97.7)	100.0 (99.9)	100.0 (100.0)
Redundancy	7.0 (7.0)	6.7 (6.5)	37.1 (37.8)
Refinement			
Resolution (Å)	52.01 – 2.19 (2.25 – 2.19)	59.95 – 1.30 (1.33 – 1.30)	71.74 – 1.42 (1.44 – 1.42)
No. reflections			
R_{work} / R_{free}	0.194/0.234	0.133/0.161	0.156/0.182
No. atoms			
Protein	19468	5234	2539
Ligand/ion	276	11	53
Water	388	700	348
B-factors			
Protein	69.0	16.5	18.8
Ligand/ion	67.9	27.3	38.6
Water	54.5	32.8	32.8
R.m.s. deviations			
Bond lengths (Å)	0.008	0.009	0.007
Bond angles (°)	1.52	1.03	1.50

Each dataset was acquired from a single crystal. Values in parentheses are for highest-resolution shell.

Supplementary Table 2. Quantitative product distribution of the enzymes reported in this study. Compounds for which a standard was not available, such as (-)-coronaridine iminium and the unknown product, could not be quantified but their occurrence is reported in the table as Detected. n.d.= not detected. Mean of three replicates ± SEM.

Enzyme	Catharanthine (nM)	Tabersonine (nM)	(-)-coronaridine iminium (nM)	Unknown product (nM)
CS				
WT	7.8 ± 1.1	n.d.	n.d.	n.d.
S172C	n.d.	n.d.	n.d.	n.d.
S172A	0.9 ± 0.6	n.d.	n.d.	n.d.
D171A, S172A	n.d.	n.d.	n.d.	n.d.
D171N, S172A	n.d.	n.d.	n.d.	n.d.
H80A	n.d.	n.d.	n.d.	n.d.
H80N	n.d.	n.d.	n.d.	n.d.
D217Y	1.0 ± 0.7	n.d.	n.d.	n.d.
Y78F	n.d.	n.d.	n.d.	n.d.
Y203F	0.2 ± 0.1	n.d.	n.d.	n.d.
Y225F	10.4 ± 1.2	n.d.	n.d.	n.d.
D273A	6.8 ± 2.4	0.6 ± 0.1	n.d.	n.d.
D273N	11.2 ± 1.0	n.d.	n.d.	n.d.
D171A	n.d.	n.d.	n.d.	n.d.
D171N	n.d.	n.d.	n.d.	n.d.
Y304F	8.4 ± 0.8	n.d.	n.d.	n.d.
F218Y	4.1 ± 1.8	n.d.	n.d.	n.d.
Loop_trim	3.7 ± 0.1	n.d.	n.d.	Detected
Loop_trim, F218Y	1.5 ± 0.2	n.d.	n.d.	Detected
Y114F	3.1 ± 2.0	n.d.	n.d.	n.d.
Helix 5 swap	3.9 ± 0.7	2.2 ± 0.1	n.d.	n.d.
Loop_trim, Helix 5 swap	1.6 ± 0.1	0.8 ± 0.1	Detected	n.d.
P173T	4.9	n.d.	n.d.	n.d.
TS				
WT	n.d.	18.4 ± 0.4	n.d.	n.d.
S170C	n.d.	19.5 ± 0.1	n.d.	n.d.
S170A	1.2 ± 0.1	0.5 ± 0.4	n.d.	n.d.
D169A	n.d.	n.d.	n.d.	n.d.
D169N	n.d.	n.d.	n.d.	n.d.
H78A	1.0 ± 0.1	7.5 ± 0.4	n.d.	n.d.
H78N	n.d.	3.4 ± 1.2	n.d.	n.d.
Y216D	n.d.	n.d.	n.d.	Detected
Y216F	n.d.	n.d.	n.d.	Detected
Loop_graft	n.d.	n.d.	n.d.	n.d.
Y76F	n.d.	n.d.	n.d.	n.d.
Y202F	n.d.	23.7 ± 2.9	n.d.	n.d.
Y224F	n.d.	20.6 ± 1.6	n.d.	n.d.
D266A	n.d.	7.0 ± 6.1	n.d.	n.d.
D266N	n.d.	20.3 ± 2.3	n.d.	n.d.
Y297F	n.d.	21.3 ± 3.7	n.d.	n.d.
Helix 5 swap	n.d.	n.d.	n.d.	Detected
Loop_graft,helix 5 swap	n.d.	n.d.	n.d.	n.d.
T171P	n.d.	2.5 ± 0.1	n.d.	n.d.
CorS				
WT	n.d.	n.d.	Detected	n.d.

Y116A	n.d.	n.d.	Detected	n.d.
S174A	2.6 ± 0.4	0.5 ± 0.4	Detected	n.d.
S174C	n.d.	11.5 ± 2.9	n.d.	n.d.
P175T	5.2 ± 0.8	2.0 ± 0.6	Detected	n.d.
T271A	n.d.	n.d.	Detected	n.d.
F300Y	n.d.	n.d.	Detected	n.d.
Helix 5 swap	n.d.	n.d.	Detected	n.d.

Supplementary Table 3. Primer sequences used in this study. Cloning overhangs are underlined. Mutated codons are in bold.

Primers for full length gene amplification	
CS_Fwd	AAGTTCTGTTTCAGGGCCCGGCTTCCCAAACTCCAACCTCAGATG A
CS_Rev	ATGGTCTAGAAAGCTTTACTCATGTTTGATGAAAGATGCTAAACG
TS_Fwd	AAGTTCTGTTTCAGGGCCCGGGTTCCTCAGATGAGACTATTTTTG
TS_Rev	ATGGTCTAGAAAGCTTTACTTGATGAAAGAAGCTAAACGTCTG
TiCorS_Fwd	AAGTTCTGTTTCAGGGCCCGGCTAATTCAACTGCAAACTCTG
TiCorS_Rev	ATGGTCTAGAAAGCTTTACTCCTTGTTGATGAAATCGC
Primers for mutagenesis	
CS_S172C_Fwd	CGATAGACTGTATTTGGCGGGTGAC**TGT**CCTGGTGCTAATATTGT TCAC
CS_S172C_Rev	GTCACCCGCCAAATACAGTCTATCG
CS_S172A_Fwd	CGATAGACTGTATTTGGCGGGTGAC**GCT**CCTGGTGCTAATATTGT TCAC
CS_S172A_Rev	Same as CS_S172C_Rev
CS_D171A_Fwd	GATTTCGATAGACTGTATTTGGCGGGT**GCC**AGTCCTGGTGCTAAT ATTGTTCAC
CS_D171A_Rev	ACCCGCCAAATACAGTCTATCGAAATC
CS_D171N_Fwd	GATTTCGATAGACTGTATTTGGCGGGT**AAC**AGTCCTGGTGCTAAT ATTGTTCAC
CS_D171N_Rev	Same as CS_D171A_Rev
CS_D171A_S172A_Fwd	GATTTCGATAGACTGTATTTGGCGGGT**GCCGCT**CCTGGTGCTAAT ATTGTTCAC
CS_D171A_S172A_Rev	Same as CS_D171A_Rev
CS_D171N_S172A_Fwd	GATTTCGATAGACTGTATTTGGCGGGT**AACGCT**CCTGGTGCTAAT ATTGTTCAC
CS_D171N_S172A_Rev	Same as CS_D171A_Rev
CS_H80A_Fwd	GAAAAACTCCCTATTTTTGTGTATGTG**GCT**GGGGCTGGCTTTTGT CTAGAATCTG
CS_H80A_Rev	CACATACACAAAAATAGGGAGTTTTTC
CS_H80N_Fwd	GAAAAACTCCCTATTTTTGTGTATGTG**AAT**GGGGCTGGCTTTTGTC TAGAATCTG
CS_H80N_Rev	CS_H80A_Rev
CS_D217Y_Fwd	CCCAACCAGCACGAAACTTAGTGAT**TAT**TTTGAGTATAACTACAC ATGTTACTG
CS_D217Y_Rev	ATCACTAAGTTTCGTGCTGGTTGGG
CS_Y78F_Fwd	GACCATGAAAAACTCCCTATTTTTGTG**TTT**GTGCATGGGGCTGGC TTTTGTCTAG
CS_Y78F_Rev	CACAAAAATAGGGAGTTTTTCATGGTC
CS_Y203F_Fwd	GTGAAAATTTTGGGGGCAATTCTTTAC**TTC**CCATATTTCATTATCC CAACCAGCACG
CS_Y203F_Rev	GTAAAGAATTGCCCCCAAAATTTTCAC
CS_Y225F_Fwd	GATGATTTTGAGTATAACTACACATGT**TTC**TGGAAATTGGCTTAT CCAAATGCTCC
CS_Y225F_Rev	ACATGTGTAGTTATACTCAAAATCATC
CS_D273A_Fwd	CCCTGGTTTCCATGATTTCAACGACTCCA**GCT**GAGACTAAAGACA TAAATGCGGTT
CS_D273A_Rev	TGGAGTCGTTGAAATCATGGAAACCAGGG
CS_D273N_Fwd	CCCTGGTTTCCATGATTTCAACGACTCCA**AAT**GAGACTAAAGACA TAAATGCGGTT
CS_D273N_Rev	Same as CS_D273A_Rev
CS_Y304F_Fwd	GGAAGTGGCTGATTTTGACGCAGAT**TTT**TTTGAACTCTTCACCTT GGAAACGG
CS_Y304F_Rev	ATCTGCGTCAAAATCAGCCACTTCC

CS_F218Y_Fwd	CAGCACGAAACTTAGTGATGAT**TAT**GAGTATAACTACACATGTTACTG
CS_F218Y_Rev	ATCATCACTAAGTTTCGTGCTG
CS_Loop_trim_Fwd	TGATTTCAACGACTCCAGATGAGACTTATATTGAGGCATTAGAAAAGAG
CS_Loop_trim_Rev	ACTCTTTTCTAATGCCTCAATATAAGTCTCATCTGGAGTCGTTGAAATC
CS_Y114F_Fwd	CCAAAGTTATTGGGGTTTCGATTGAA**TTT**AGACTTGCCCCAGAGCACCTTTTAC
CS_Y114F_Rev	TTCAATCGAAACCCCAATAACTTTGG
CS_Helix 5_swap_Fwd	CCCATATTTCATTATCCCAACCAGCACGAAA**CAGAGTGATTATATGGAGAATGAGTATAGATCT**TACTGGAAATTGGCTTATCCAAATGCTCC
CS_Helix 5_swap_Rev	TTTCGTGCTGGTTGGGATAATGAAATATGGG
CS_P173T_Fwd	CGATAGACTGTATTTGGCGGGTGACAGT**ACT**GGTGCTAATATTGTTCACAACACAC
CS_P173T_Rev	ACTGTCACCCGCCAAATACAGTCTATCG
TS_S170C_Fwd	CGATAGACTCTATTTGTGGGGTGAT**TGC**ACCGGTGCCAATATTGTTCACAACAC
TS_S170C_Rev	ATCACCCCACAAATAGAGTCTATCG
TS_S170A_Fwd	CGATAGACTCTATTTGTGGGGTGAT**GCC**ACCGGTGCCAATATTGTTCACAACAC
TS_S170A_Rev	Same as TS_S170C_Rev
TS_D169A_Fwd	GATTTCGATAGACTCTATTTGTGGGGT**GCT**TGCACCGGTGCCAATATTGTTCACAA
TS_D169A_Rev	ACCCCACAAATAGAGTCTATCGAAATC
TS_D169N_Fwd	GATTTCGATAGACTCTATTTGTGGGGT**AAT**TGCACCGGTGCCAATATTGTTCACAA
TS_D169N_Rev	Same as TS_D169A_Rev
TS_H78A_Fwd	GAAAAACTCCCCATTATAGTCTATTTC**GCT**GGAGCTGGTTTTTGTCTTGAATCGG
TS_H78A_Rev	GAAATAGACTATAATGGGGAGTTTTTC
TS_H78N_Fwd	GAAAAACTCCCCATTATAGTCTATTTC**AAT**GGAGCTGGTTTTTGTCTTGAATCGG
TS_H78N_Rev	Same as TS_H78A_Rev
TS_Y216D_Fwd	CAGGACGAGTTCAAAACAGAGTGAT**GAT**ATGGAGAATGAGTATAGATCTTACTG
TS_Y216D_Rev	ATCACTCTGTTTTGAACTCGTCCTG
TS_Y216F_Fwd	CAGGACGAGTTCAAAACAGAGTGAT**TTT**ATGGAGAATGAGTATAGATCTTACTG
TS_Y216F_Rev	Same as TS_Y216D_Rev
TS_Loop_graft_Fwd	CTCGAGGTTGCTGATTTCCATGGTTGCC**ATGATTTCAACGACTCCA**GATGAAGCTAGAGATATAACTCTTC
TS_Loop_graft_Rev	GGCAACCATGGAAATCAGCAACCTCGAG
TS_Y76F_Fwd	CATGATGAAAAACTCCCCATTATAGTC**TTT**TTCCATGGAGCTGGTTTTTGTCTTG
TS_Y76F_Rev	GACTATAATGGGGAGTTTTTCATCATG
TS_Y202F_Fwd	GTGAAGATTTTGGGGGCAATTCTTTAC**TTC**CCATATTTCTTAATCAGGACGAGTTC
TS_Y202F_Rev	GTAAAGAATTGCCCCCAAAATCTTCAC
TS_Y224F_Fwd	GATTATATGGAGAATGAGTATAGATCT**TTC**TGGAAATTGGCTTACCCAGATGCTCC
TS_Y224F_Rev	AGATCTATACTCATTCTCCATATAATC
TS_D266A_Fwd	CGAGGTTGCTGATTTCCATGGTTGCC**GCT**GAAGCTAGAGATATAACTCTTCTTTA
TS_D266A_Rev	GGCAACCATGGAAATCAGCAACCTCG
TS_D266N_Fwd	CGAGGTTGCTGATTTCCATGGTTGCC**AAT**GAAGCTAGAGATATAACTCTTCTTTA
TS_D266N_Rev	Same as TS_D266A_Rev

TS_Y297F_Fwd	TAGATGTGGCTGATTTTGATAAACAG**TTT**TTTGAACTGTTTGAAATGGAAACAG
TS_Y297F_Rev	CTGTTTATCAAAATCAGCCACATCTA
TS_Helix 5_swap_Fwd	CTTAATCAGGACGAGTTCAAAACAGAGTGAT**GATTTTGAGTATAACTACACATGT**TACTGGAAATTGGCTTACCCAGATGCTCC
TS_Helix 5_swap_Rev	ATCACTCTGTTTTGAACTCGTCCTGATTAAG
TS_Loop_graft_Fwd	CTCGAGGTTGCTGATTTCCATGGTTGCC**ATGATTTCAACGACTCC**AGATGAAGCTAGAGATATAACTCTTC
TS_Loop_graft_Rev	GGCAACCATGGAAATCAGCAACCTCGAG
TS_T171P_Fwd	CGATAGACTCTATTTGTGGGGTGATAGC**CCC**GGTGCCAATATTGTTCACAACACACTTATC
TS_T171PF_Rev	GCTATCACCCCACAAATAGAGTCTATCG
CorS_Y116F_Fwd	GCTGTCGGAGTTTCGGTTGAG**TTT**AGACTCGCCCCCGAGCACCC
CorS_Y116F_Rev	CTCAACCGAAACTCCGACAGC
CorS_S174A_Fwd	CAATAAGCTTTACTTGGGTGGTGAC**GCG**CCTGGTGGAAATATTGTGCAC
CorS_S174A_Rev	GTCACCACCCAAGTAAAGCTTATTG
CorS_S174C_Fwd	CAATAAGCTTTACTTGGGTGGTGAC**TGC**CCTGGTGGAAATATTGTGCAC
CorS_S174C_Rev	GTCACCACCCAAGTAAAGCTTATTG
TiCorS_P175T_Fwd	CTTTACTTGGGTGGTGACAGT**ACC**GGTGGAAATATTGTGCACAACG
CorS_P175T_Rev	ACTGTCACCACCCAAGTAAAG
CorS_T271A_Fwd	GTTTCCATGGTTTCGGACGAG**GCG**AGAGATATAACCCTTCTCTAC
CorS_T271A_Rev	CTCGTCCGAAACCATGGAAAC
CorS_F300Y_Fwd	GTGGGTGACTACGAAGCACAT**TAT**TTTGATTTGTTCAGCCCTGAAAATG
CorS_F300Y_Rev	ATGTGCTTCGTAGTCACCCAC
CorS_Helix 5_swap_Fwd	CAAGCAAAAGACAGAGTGAT**GATTTTGAGTATAACTACACATGT**TACTGGAAGTTGGCTTATCCATC
CorS_Helix 5_ swap_Rev	ATCACTCTGTCTTTTGCTTG

Supplementary Table 4. MRM transitions used for metabolites detection with UPLC/QqQ-MS method.

Compound	Parent ion	Daughter ion	Collision Energy (V)
Catharanthine	337.2	173.1	16
		165.1	20
		144.1	20
Tabersonine	337.2	305.2	22
		228.2	22
		168.1	36
Coronaridine	339.2	144.2	30
		307.2	30
Angryline	337.2	122.0	20
		168.1	36
		228.0	20
16-carbomethoxy-cleaviminium	337.2	136.1	24
		168.1	36
		305.1	22
16-carbomethoxy-cleavamine	339.2	130.1	30
		144.2	30
Stemmadenine acetate	397.2	337.1	18
		228.1	24
		168.0	40
Precondylocarpine acetate	395.2	234.0	38
		228.1	22
		196.1	32

Supplementary Figures

Supplementary Fig. 1. Examples of aspidosperma and iboga alkaloids.

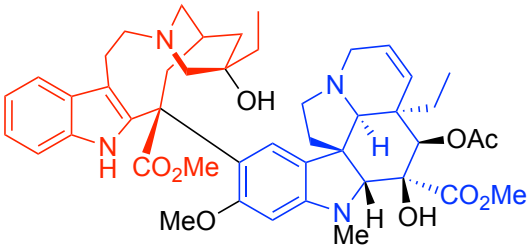

Vinblastine
anti-cancer

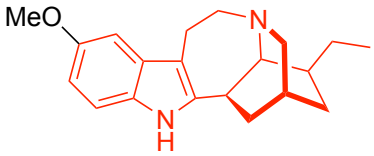

Ibogaine
anti-addiction

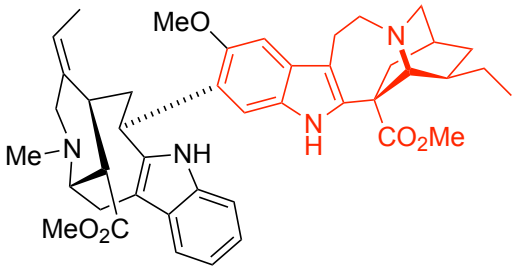

Voacamine
anti-malarial

Supplementary Fig. 2. Dehydrosecodine enamine **3b**, which has a dihydropyridine moiety (green) and methyl acrylate (purple) moiety which can undergo one of two formal Diels-Alder reactions to form either (+)-catharanthine **4** or (–)-tabersonine **5**.

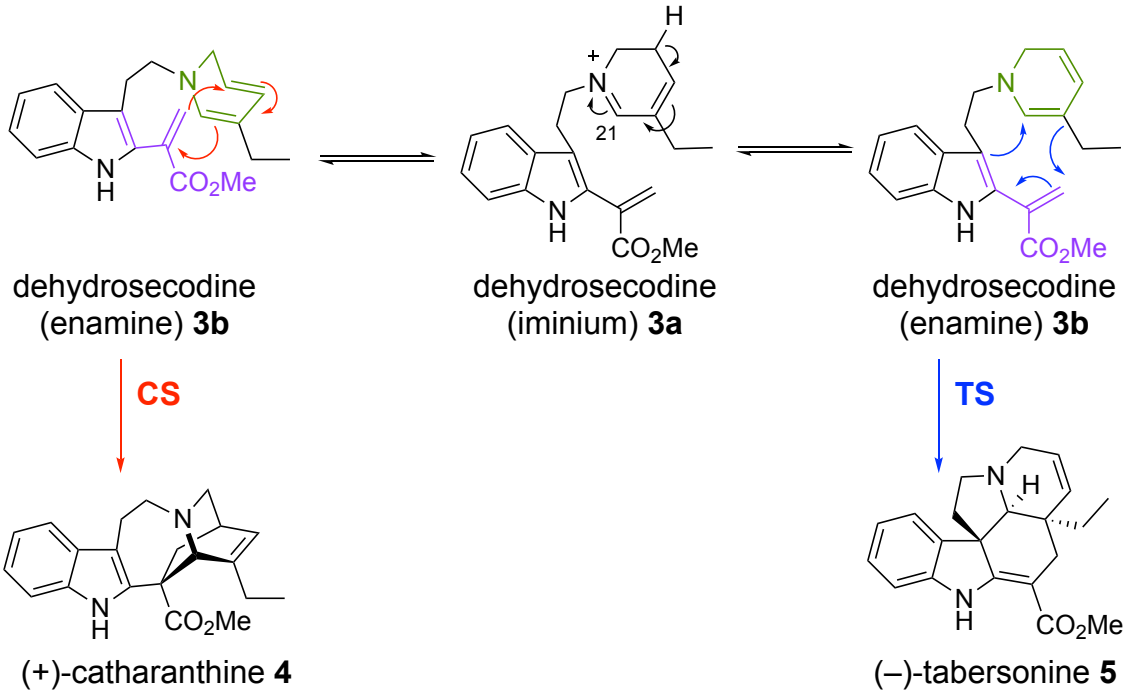

Supplementary Fig. 3. Structure-based sequence alignment of TS (GenBank: MF770513), CorS (GenBank:MK840854) and CS (GenBank: MF770512). The secondary elements of the enzymes are presented at the top and at the bottom. The gray box shows the N-terminal β-flap; the purple box highlights the Ala-Gly residues that replace the oxyanion hole of canonical carboxylesterases; the cyano box highlights the GXSXG motif in which the catalytic Ser of the carboxylesterases is located; the green box shows the portion of helix 5 used for the swaps; the blue box shows the extended loop occurring only in CS. The grey arrow indicates the catalytic Asp of canonical carboxylesterases. This figure was generated using ESPript3.0 (Robert, X. & Gouet, P. *Nucleic Acid Res*. **42**, W320-324 (2014)).

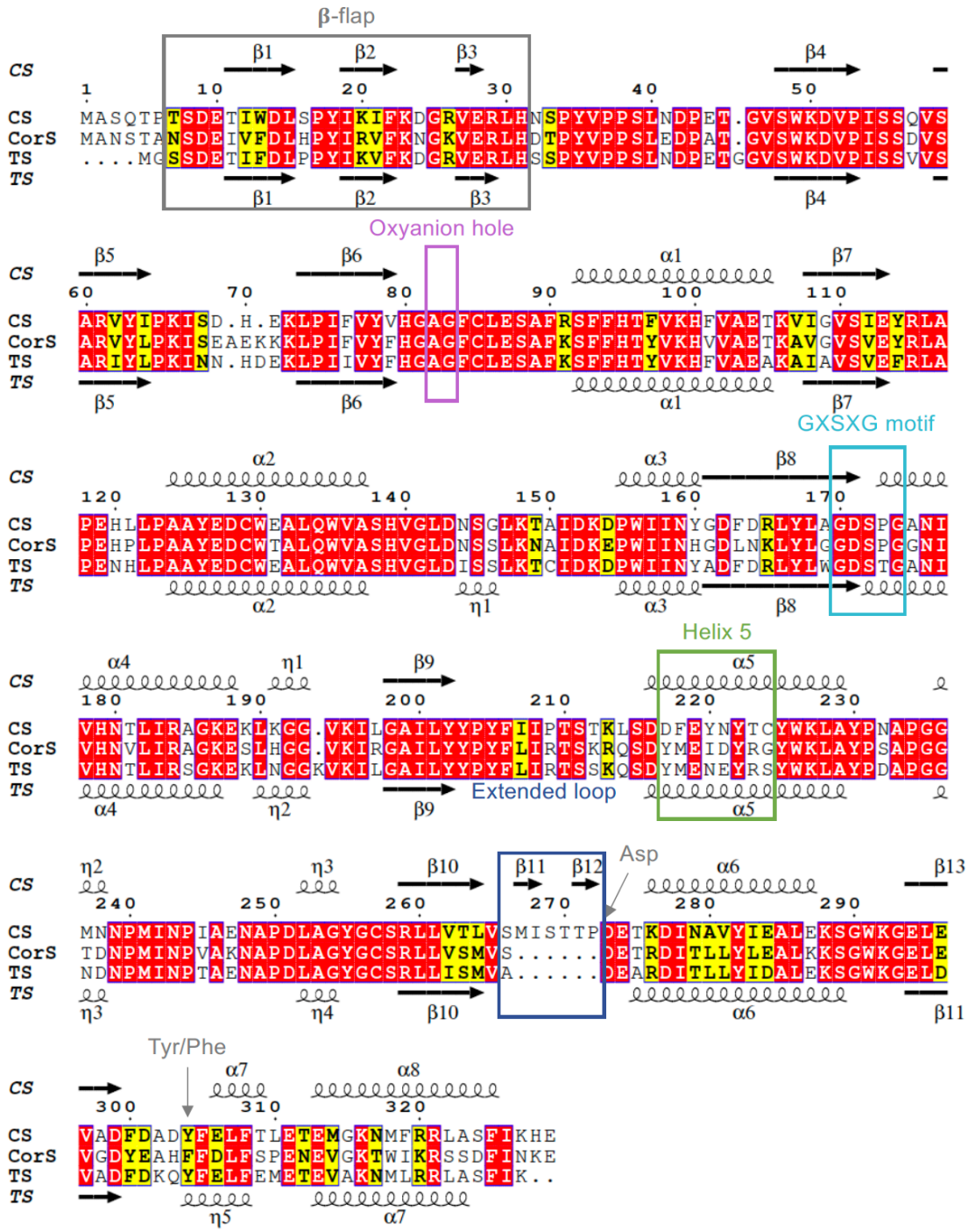

Supplementary Fig. 4. HRMS and MS/MS spectra of angryline **3c**. Angryline formula: $C_{21}H_{25}N_2O_2^+$; Theoretical mass: 337.1911; Observed mass: 337.1917; error: 1.8 ppm.

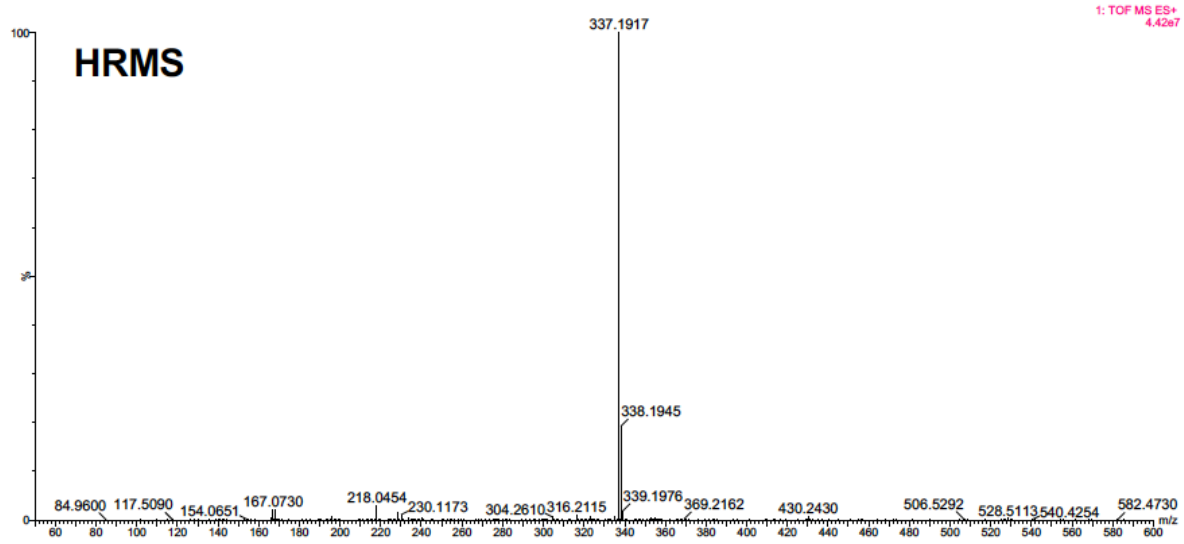

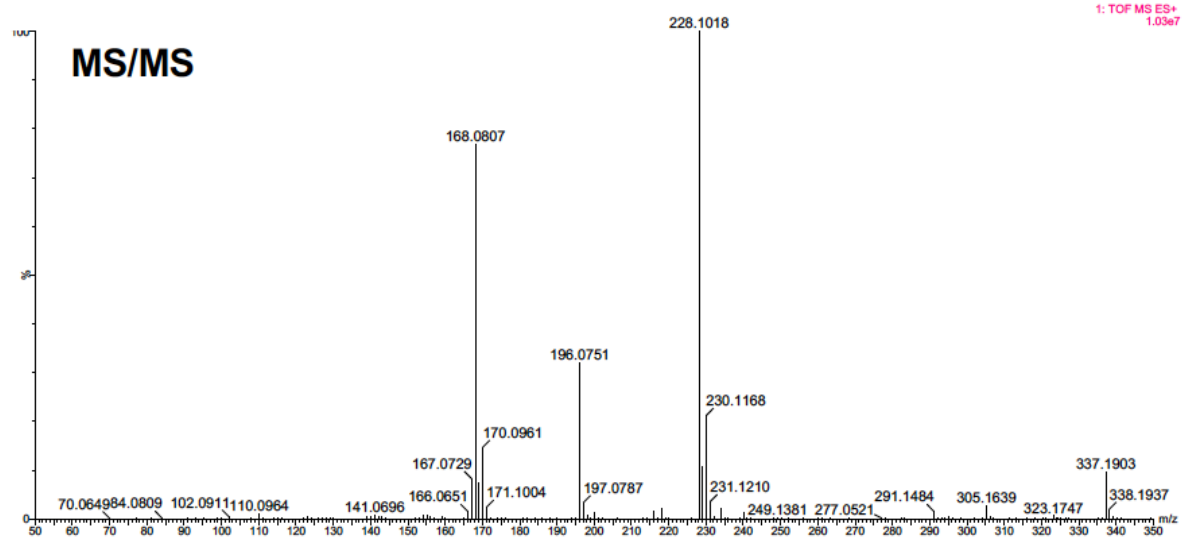

Supplementary Fig. 5. Degradation of angryline **3c**. **a**) Product profile of DPAS-catalyzed reaction. The stars indicate unknown by-products formed during the reaction. **b**) Degradation of angryline at pH 9.5. This assay was performed at 37 °C.

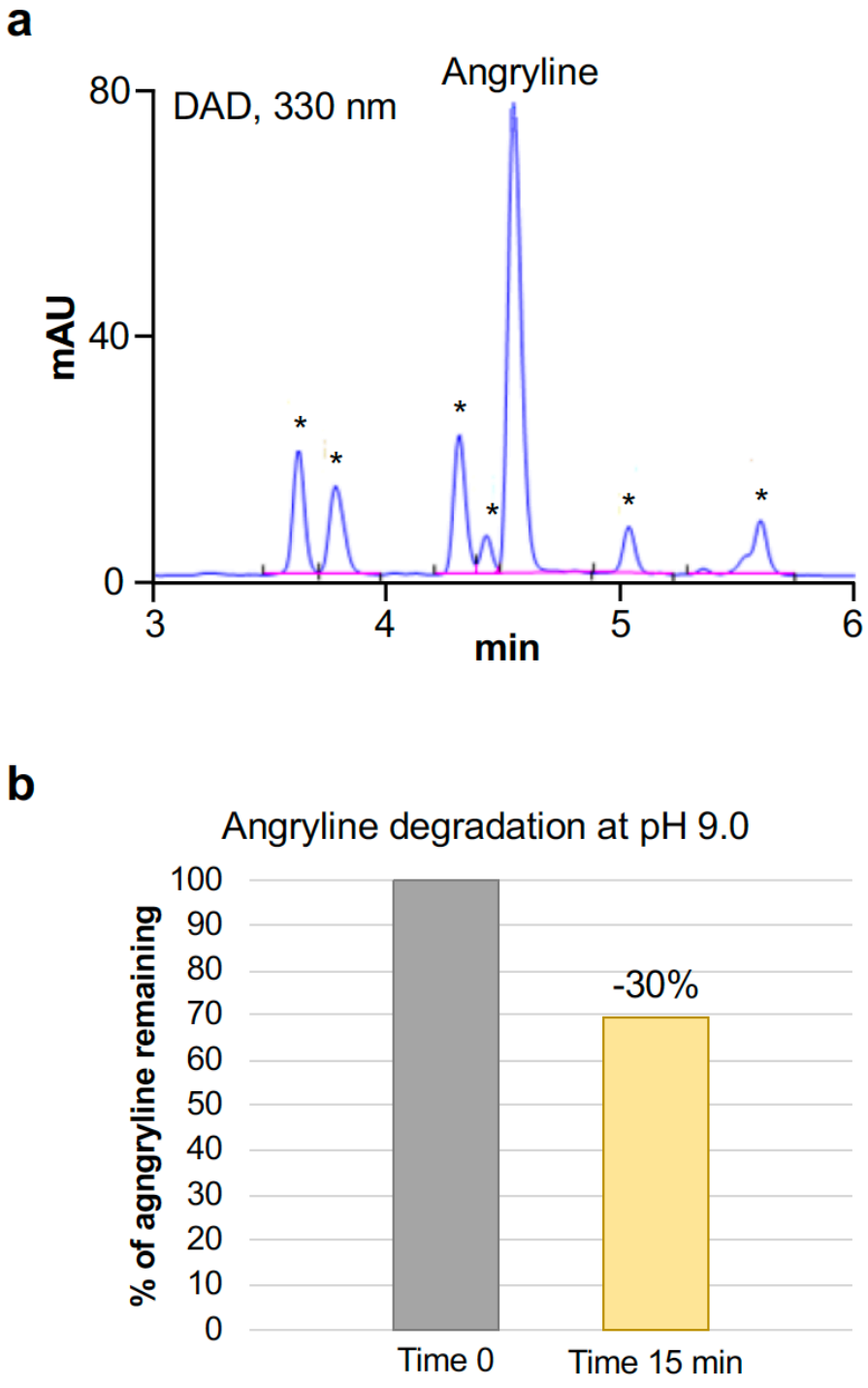

Supplementary Fig. 6. CD spectrum of angryline **3c** (1 mM) in 100 mM MES buffer pH 6.0.

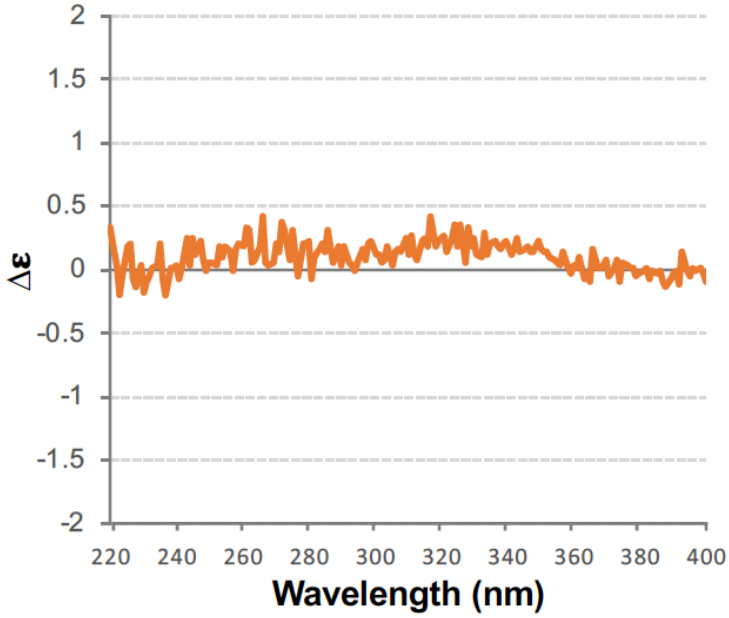

Supplementary Fig. 7. Activity of CS and TS using angryline **3c** as substrate. Formation of catharanthine **4** and tabersonine **5** were monitored. Reactions were performed in CHES buffer pH 9.5 and incubated at 37 °C for 20 min. Black lines display time 0; red lines display time 20 min. The total ion count of the MRMs for the different compounds is displayed in the retention time windows in which the compounds elute.

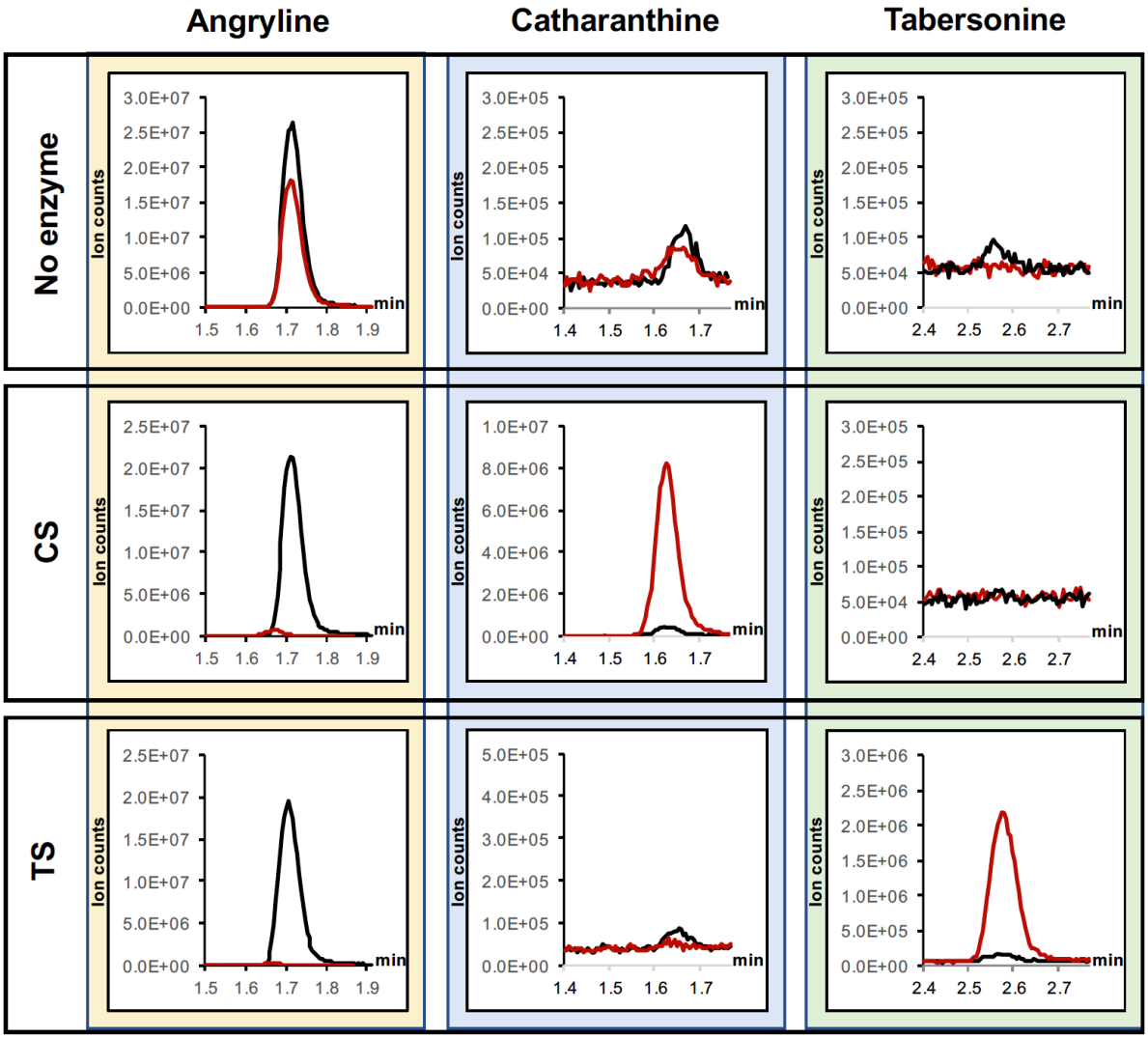

Supplementary Fig. 8. pH dependence of CS and TS reactions. **a)** Consumption of angryline **3c** over 20 minutes at 37 °C at different pH. **b)** and **c)** Activity of CS and TS using angryline **3c** as substrate, measuring formation of catharanthine **4** and tabersonine **5**. Reactions were performed for 20 min at 37 °C at different pH. CS specific activity at pH 9.5 was 766 pmol/min/mg; TS specific activity at pH 9.5 was 260 pmol/min/mg.

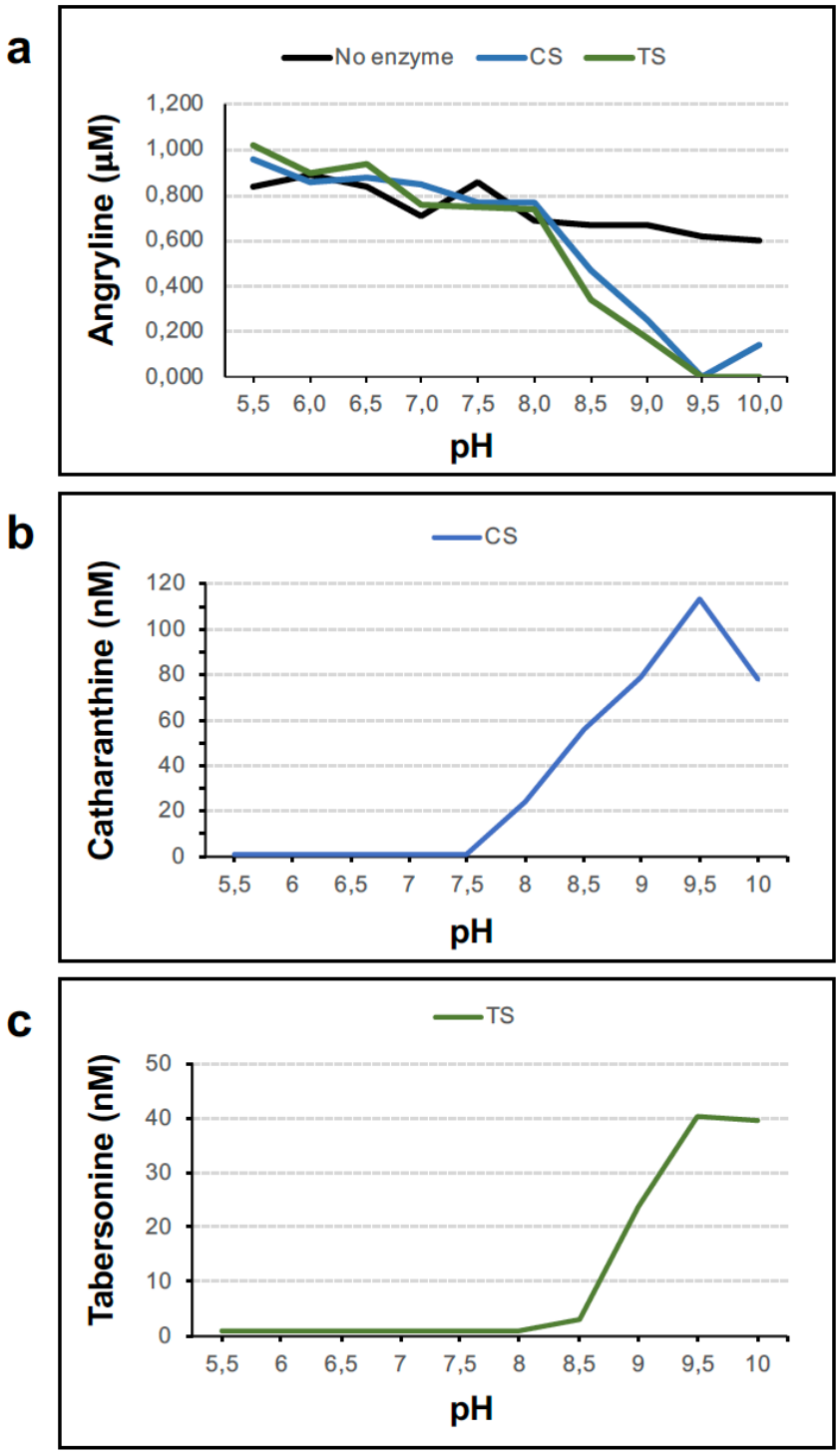

Supplementary Fig. 9. Proposed mechanism of formation of the more stable dehydrosecodine isomer angryline **3c**. Under acidic conditions, the equilibrium favors the formation of angryline, while at neutral pH, dehydrosecodine likely exists as the enamine tautomer **3b**, which can undergo a cycloaddition reaction, potentially through a Diels-Alder reaction.

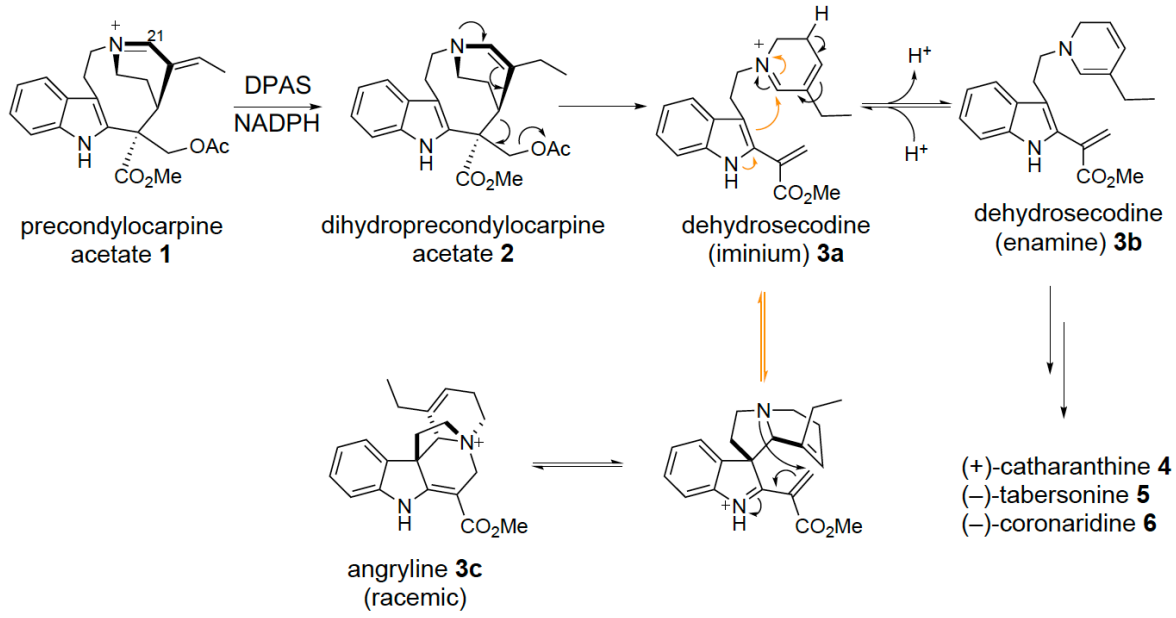

Supplementary Fig. 10. Comparison of CS, TS and CorS homodimers. For each structure, orthogonal views are depicted in cartoon representation, where the left-hand subunit is shown in rainbow coloration from blue at the N-terminus through to red at the C-terminus, and the right-hand subunit is in grey; the active site Ser residues are marked by black spheres. **a)** CS homodimer, of which there are four in the asymmetric unit (ASU) with dimer interface areas in the range 950-967 Å^2, as calculated by the jsPISA server (http://www.ccp4.ac.uk/pisa; Krissinel, E. *Nucleic Acids Res*. **43**, W314-319 (2015)). Pairwise superpositions of subunits give rmsd values in the range 0.107-0.495 Å, and for dimers, values in the range 0.260-0.450 Å are obtained. **b)** TS homodimer, which corresponds to the ASU, giving a dimer interface area of 1290 Å^2; the two subunits superpose with an rmsd value of 0.612 Å. **c)** CorS homodimer generated through the application of 2-fold crystallographic symmetry to the ASU, which comprises a single CorS subunit. The resultant dimer interface area is 1198 Å^2. In pairwise comparisons of the three structures, superpositions of subunits (A chain only) then dimers (A-B dimers for CS and TS, and A-A dimer for CorS) gave rmsd values of 1.045 and 1.136 Å for CS vs. TS, 1.177 and 1.188 for CS vs. CorS, and 1.104 and 1.156 for TS vs. CorS, respectively.

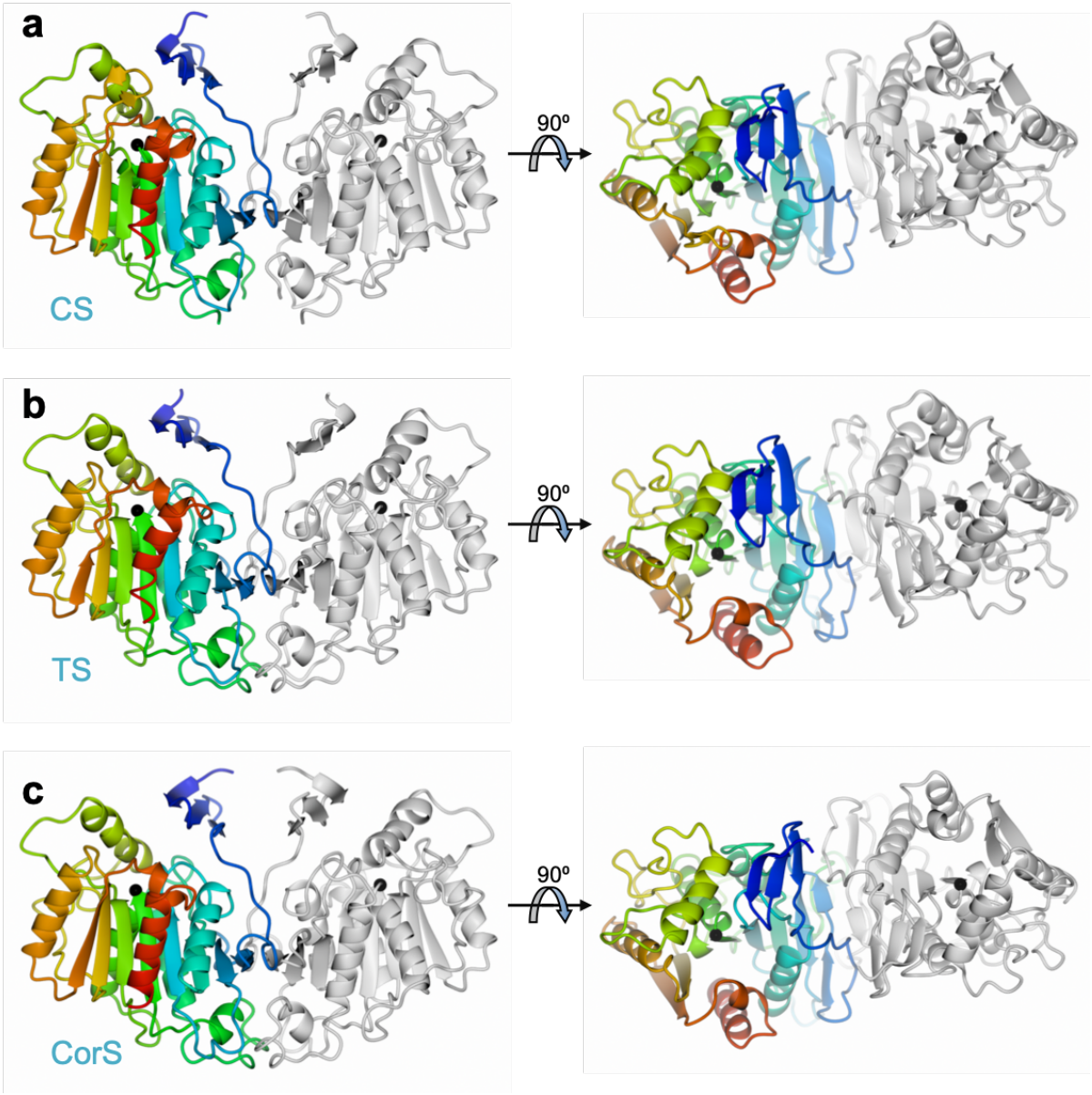
a
CS
90º
b
TS
90º
c
CorS
90º

Supplementary Fig. 11. Comparison of the TS catalytic triad with the canonical Ser-His-Asp catalytic triad from the *Actinidia eriantha* carboxylesterase (AeCXE1), with which it shares 29% sequence identity. After superposing the structures (with RMSD 1.898 Å), it is clear that the separation between the Ser and Asp Cα atoms is significantly longer in TS (blue cartoon and carbons) than it is in AeCXE1 (brown cartoon and carbons), such that a TS Y297H substitution would be unlikely to reconstitute the hydrogen bonding network necessary to activate the Ser for nucleophilic attack, without a rearrangement of the protein backbone. The corresponding Cα-Cα distances are 12.5 Å and 13.3 Å for CS and CorS, respectively.

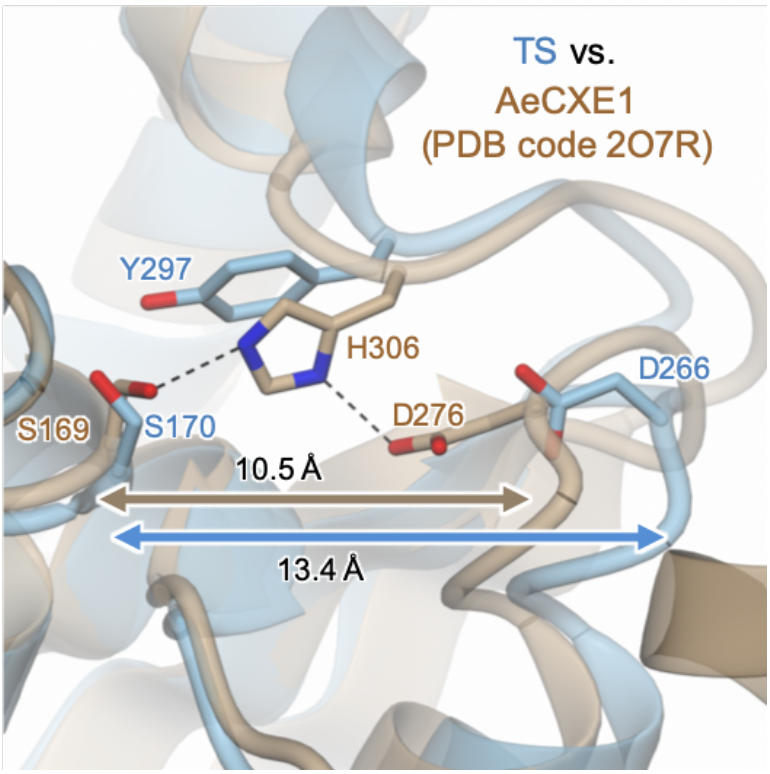

Supplementary Fig. 12. Comparison of oxyanion holes for CS, TS and CorS. **a)** CS with the 16-carbomethoxycleaviminium **7** intermediate bound (see main text and Supplementary Fig. 11), **b)** TS with docked dehydrosecodine **3b** (substrate; top) and tabersonine **5** (product; bottom), and **c.** CorS with docked dehydrosecodine **3b** (substrate; top) and coronaridine iminium **9** (product; bottom). The view corresponds approximately to that used for Figure 2c-e with a small rotation around the vertical axis. The backbone trace of the nucleophilic elbow (foreground; brown) and the oxyanion hole loop (background; pale blue) are shown in cartoon and key residues are in stick representation with yellow carbons. Ligands are shown as sticks with green carbons and also depicted as a 2D representation at the top of each panel. In both representations, the two C-C bonds that form as a result of catalysis are indicated by spheres of the same colour for each bond (i.e. black or white). In all cases, the carbonyl oxygen of the methyl acrylate group in the ligand interacts with the oxyanion hole, which is governed by the shape of the molecular surface in this region and is illustrated by semi-transparent van der Waals spheres covering the adjacent protein atoms. In CS and CorS, where the residue directly after the catalytic Ser is a Pro, the surface is comparatively flat here and the interaction is somewhat superficial. However, in TS the Pro is substituted by a Thr, which results in a distinct hole in the molecular surface that can accommodate the carbonyl oxygen. Moreover, the Thr is able to provide additional hydrogen bonding potential to the oxygen via its main-chain nitrogen and side-chain hydroxyl. As a result, the methyl acrylate group is more deeply engaged than in the other two active sites. Further, a hydrogen bond between Ser170 and the indole nitrogen may assist in keeping the indole group and the methyl acrylate moiety of dehydrosecodine **3b** roughly in the same plane in TS, which may be important for guiding catalysis towards tabersonine **5** rather than catharanthine **4**.

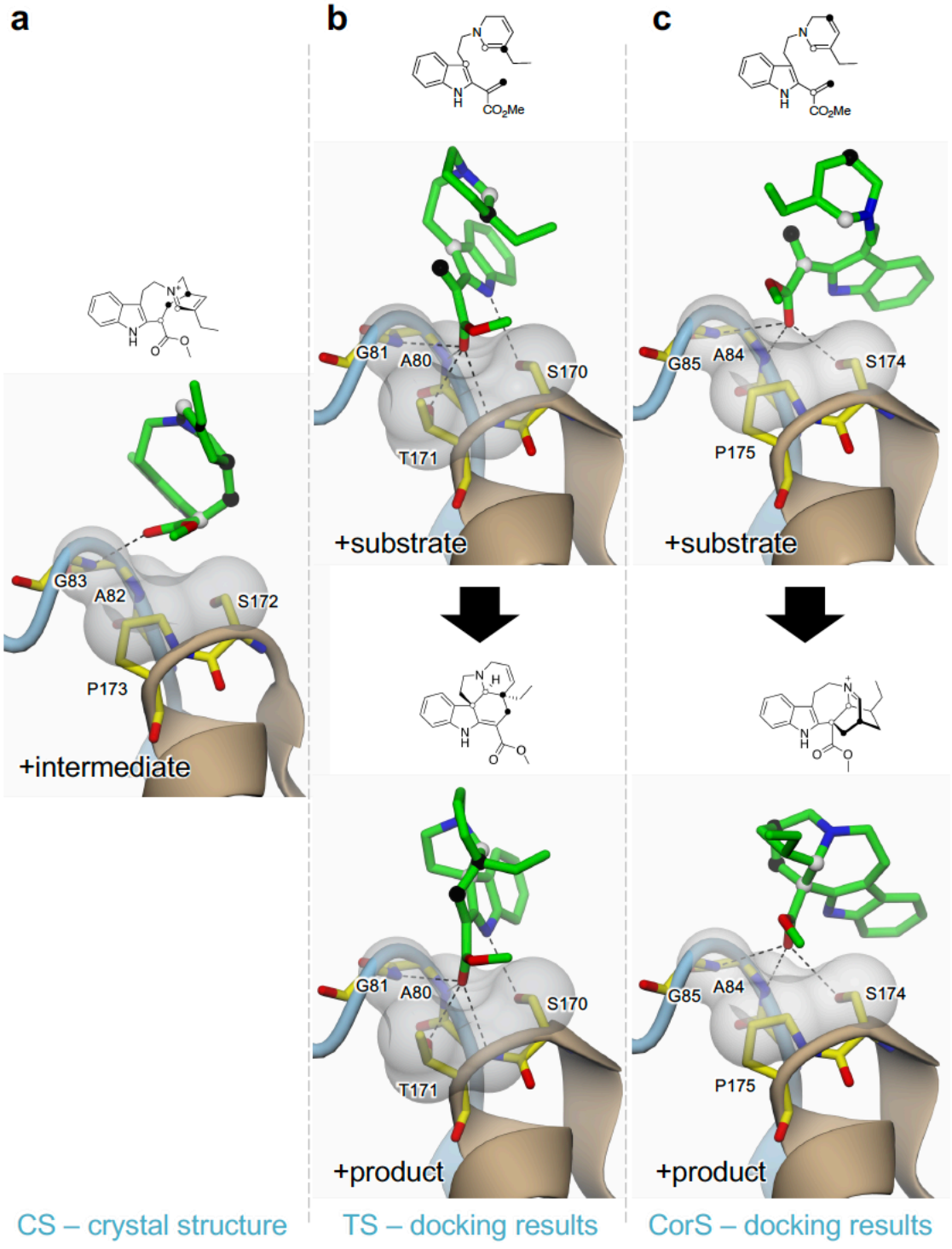
a
b
c
G83
A82
S172
P173
+intermediate
G81
A80
S170
T171
+substrate
G85
A84
S174
P175
+substrate
G81
A80
S170
T171
+product
G85
A84
S174
P175
+product
CS – crystal structure
TS – docking results
CorS – docking results

Supplementary Fig. 13. Hydrolytic activity of CS, TS and TS Y297H towards the model substrate umbelliferyl butyrate. No substrate consumption was observed after incubation at 37 °C for 2 h.

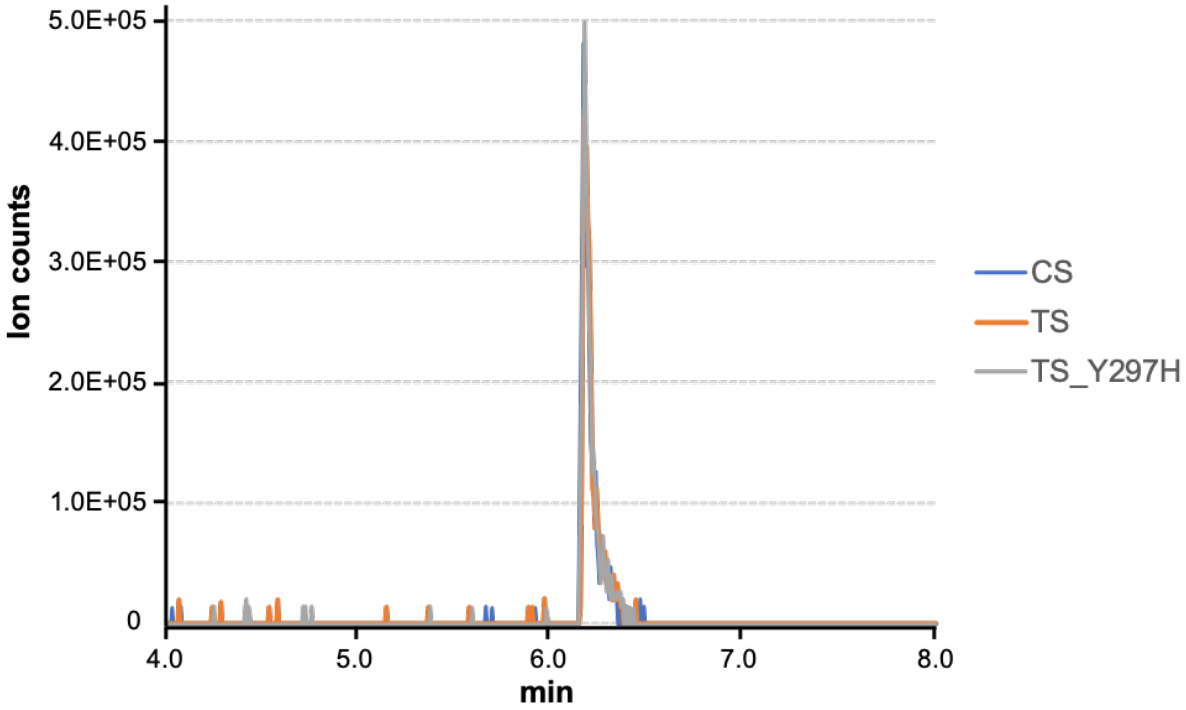

Supplementary Fig. 14. Crystallographic evidence supporting the assignment of the cleaviminium intermediate **7** bound in the active site of CS. Despite being co-crystallized with the product catharanthine **4**, the X-ray data indicate that the intermediate is present. The stereoviews below display 2.2 Å resolution omit mF_{obs}-DF_{calc} difference electron density for the bound ligand calculated using phases from the final model without the ligand after the application of small random shifts to the atomic coordinates, re-setting temperature factors, and re-refining to convergence (rendered at two contour levels: 2.5σ in blue mesh, and 5.0σ as a semi-transparent pink surface). The ligand is highlighted with green carbons, and residues from the catalytic triad and oxyanion hole with yellow carbons; the protein backbone trace is depicted as a semi-transparent pale blue cartoon. (**a**) The cleaviminium could be confidently built into density at the active sites of each of the eight CS subunits that comprise the asymmetric unit. After refinement, the RSCC values provided by the PDB validation server (https://validate.wwpdb.org/) were in the range 0.91-0.98, indicative of a good fit. Moreover, refinement with the ligand present gave negligible residual difference electron density (not shown). (**b**) The enamine form of the substrate dehydrosecodine **3b** also fitted the omit density well and similarly gave negligible residual difference electron density after refinement (not shown). However, the equivalents of the two carbon atoms that become covalently linked in the intermediate refine to interatomic distances in the range 2.25-2.71 Å (double-headed dotted arrow), which are significantly shorter than twice the van der Waals radius of carbon (i.e. 3.4 Å), indicating that they should be linked together. Re-refining with the interatomic distance restrained to 3.0 Å resolution resulted in a positive difference density peak between the two atoms (not shown), again suggesting that they should be linked. (**c**) The fit with catharanthine **4** was significantly worse, with some atoms out of density and not all of the strong density accounted for. After refinement with the ligand present, these issues were highlighted by strong peaks of both positive and negative difference electron density (bottom).

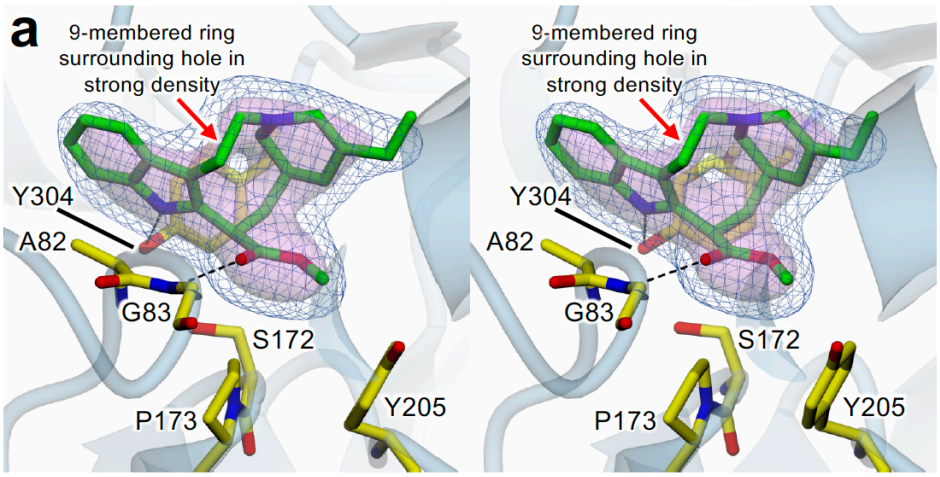

16-carbomethoxycleaviminium

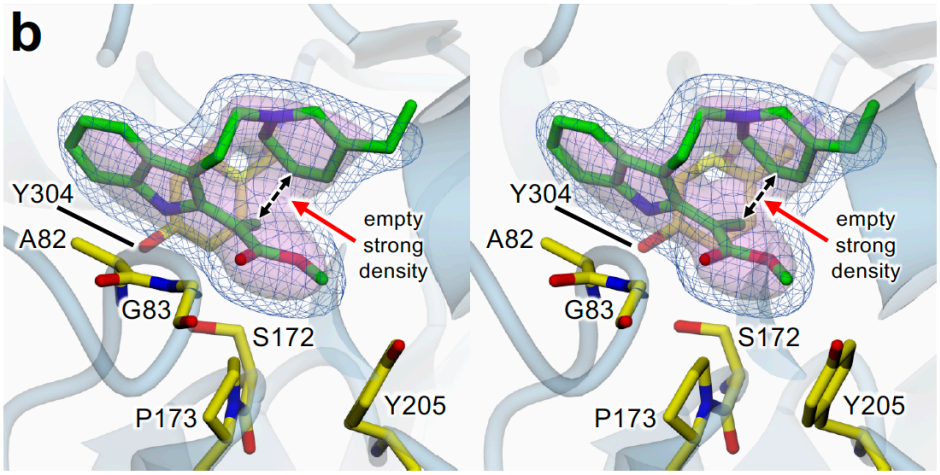

dehydrosecodine (enamine)

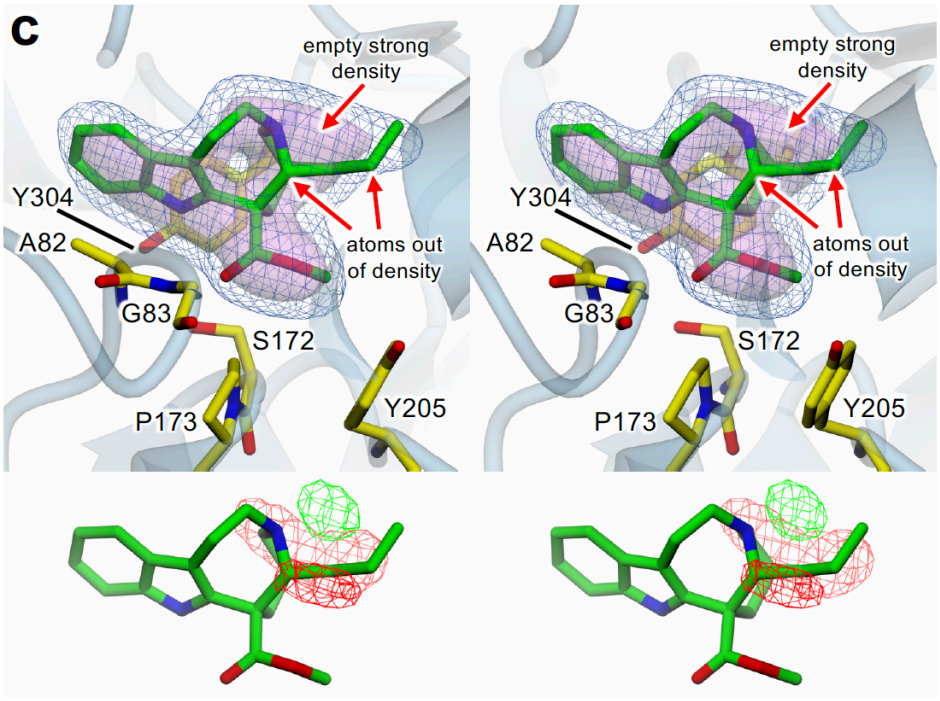

catharanthine

Supplementary Fig. 15. Possible cyclization mechanisms. **a.** Retro-Mannich opening of (+)-catharanthine **4** leads to 16-carbomethoxycleavamine **8** via 16- carbomethoxycleaviminium **7**. It appears from the crystal structure that the keto form of **7**, with *R* stereochemistry at C16, is bound in the active site. **b.** Stepwise cyclization in the forward direction to form (+)-catharanthine **4**. **c.** Cyclization to form (–)-tabersonine **5** could proceed step-wise or through a concerted Diels-Alder reaction. **d.** Tautomerization, followed by aza Diels-Alder cyclization to form (–)-coronaridine **6**.

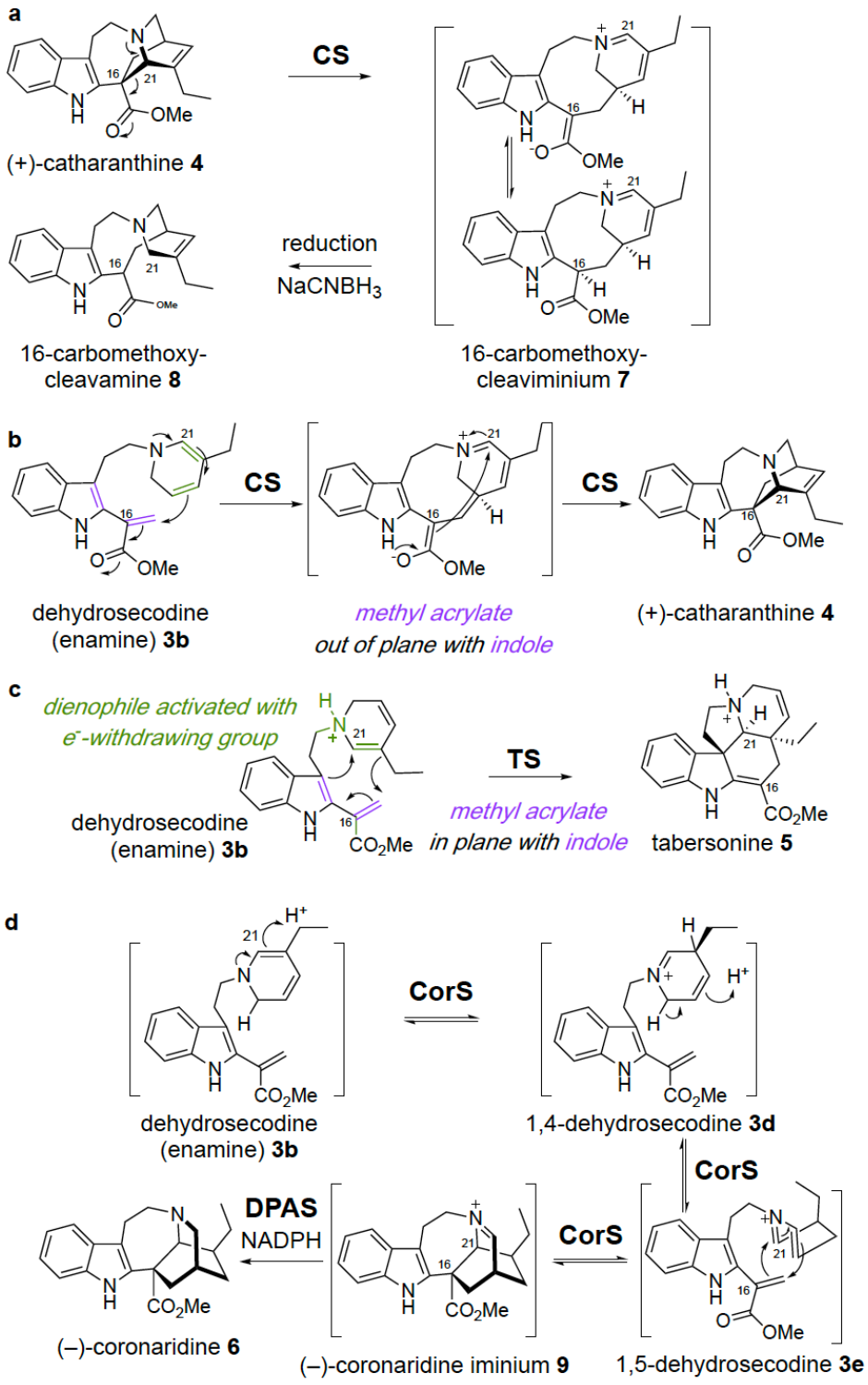

Supplementary Fig. 16. Formation of 16-carbomethoxycleaviminium **7** from catharanthine **4**. **a)** Reaction performed by CS at 37 °C for 24 h. **b)** Incubation of catharanthine **4** with trifluoroacetic acid for 1 h. **c)** Reduction of the CS product with sodium cyanoborohydride to form 16-carbomethoxycleavamine **8**. **d)** Reduction of the TFA product with sodium cyanoborohydride. The total ion count of the MRMs for the different compounds is displayed.

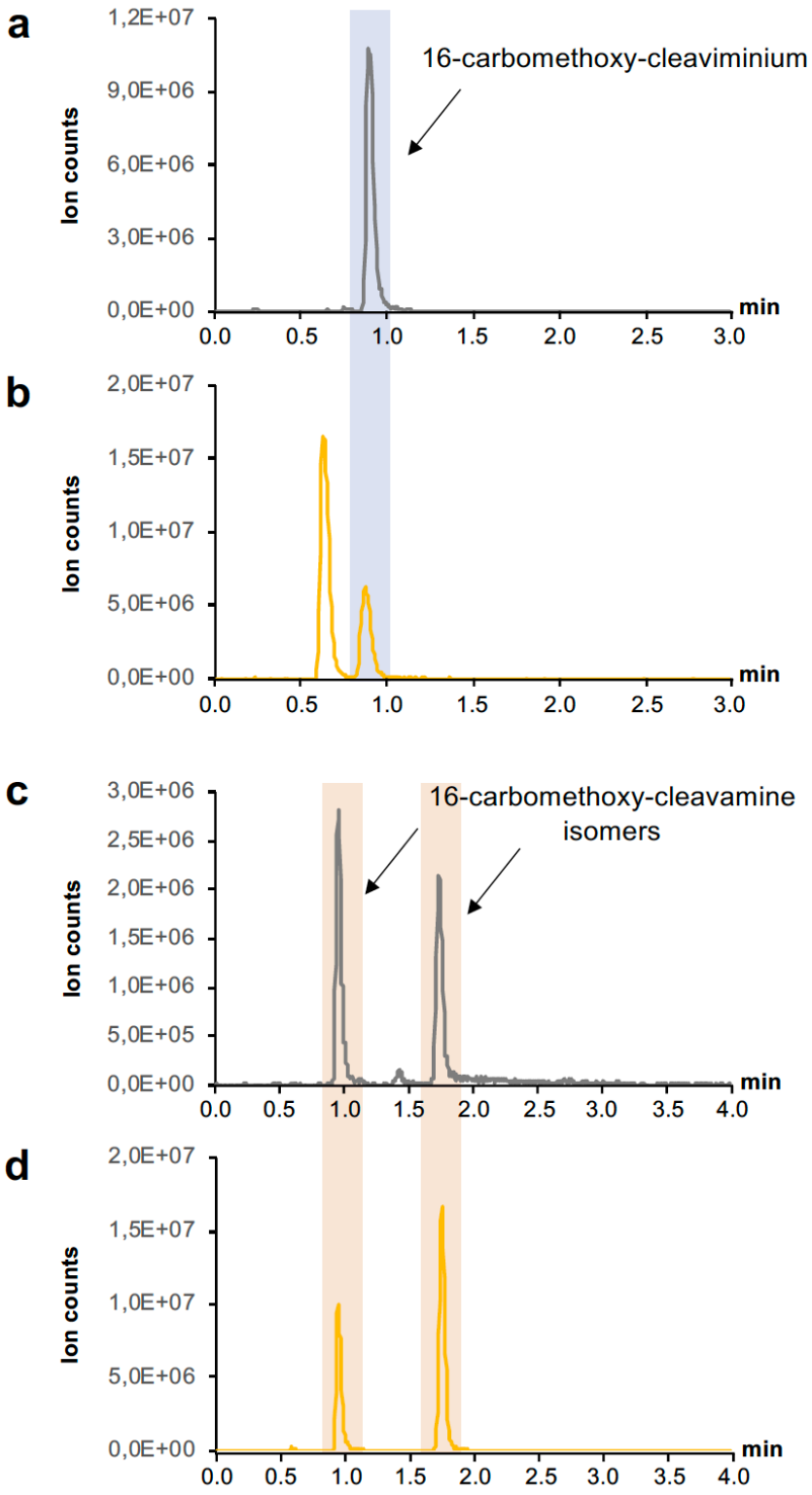

Supplementary Fig. 17. Comparison of active site cavities for CS, TS and CorS subunits. Throughout, the view corresponds to a top view with respect to Figure 2a. Each structure is shown in rainbow coloration from blue at the N-terminus through to red at the C-terminus, where the left-hand panels show a cartoon representation, and the right-hand panels show a molecular surface; ligands are shown as sticks with green carbons and the positions of catalytic triad residues are marked by black spheres and labelled with single-letter amino acid codes. **a)** CS with the cleaviminium intermediate **7** bound, which shows the most enclosed active site, this being due, in part, to the extended loop that is absent from the other two. **b)** TS with docked tabersonine **5**, which displays a relatively exposed active site that could be mechanistically important (see main text). **c)** CorS with docked coronaridine iminium **9**, showing an active site that is intermediate between CS and TS in terms of exposure to solvent.

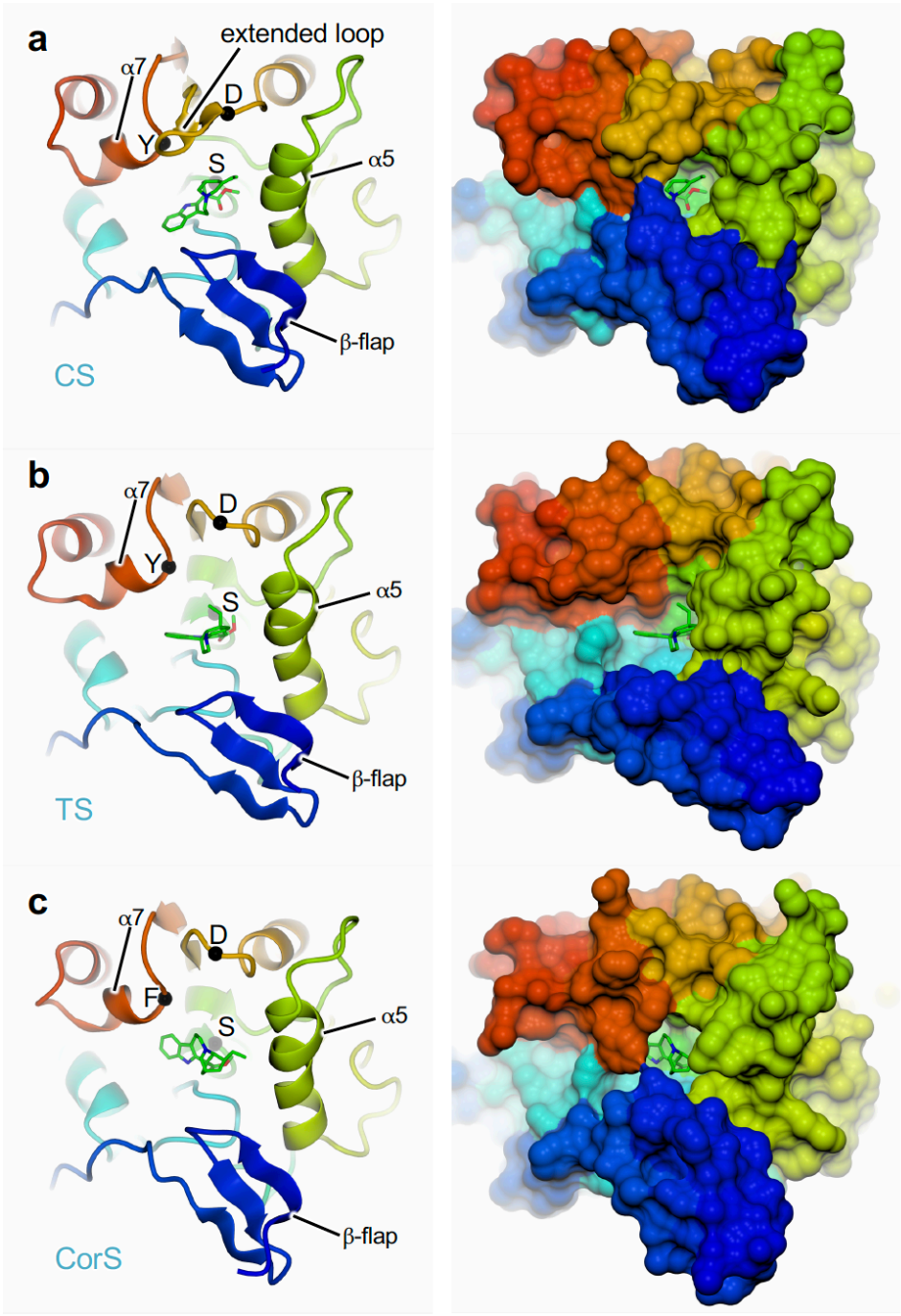

Supplementary Fig. 18. Activity of mutant TS S170A using angryline **3c** as substrate. Reactions were performed at pH 9.5 for 20 min at 37 °C. **a)** Shows that TS S170A is able to form catharanthine **4** whilst the wild type enzyme is not. **b)** Shows that the mutant still retains the ability to form tabersonine **5**, although it is less active. The total ion count of the MRMs for the different compounds is displayed in the retention time windows in which the compounds elute.

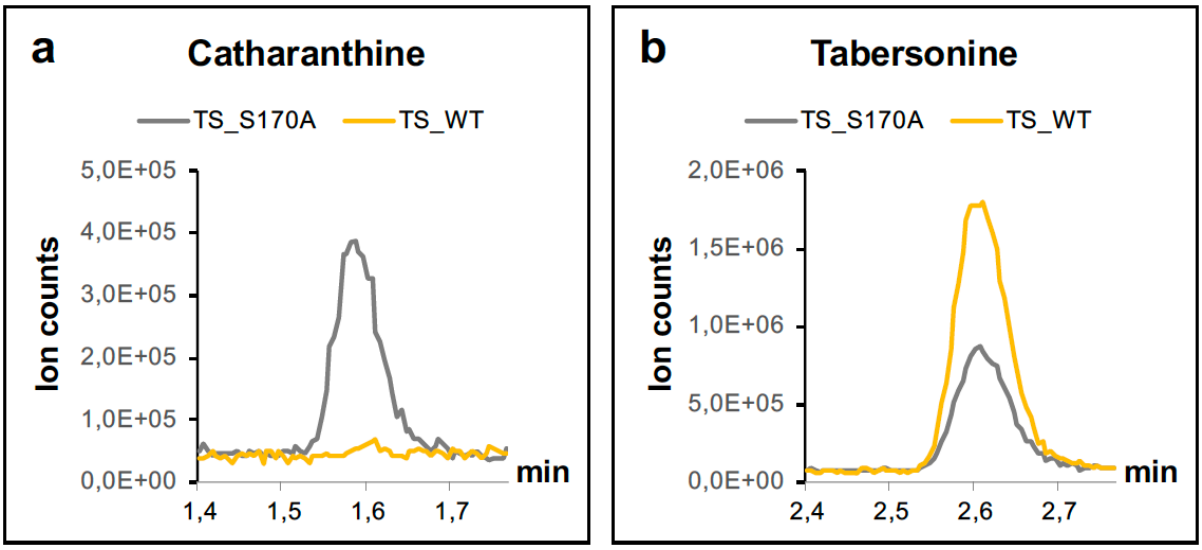

Supplementary Fig. 19. Residues targeted in the mutational analysis of CS. Amino acid residues targeted in this study are shown with yellow carbons. The loop in brown is unique to CS and was trimmed. Helix α5 is highlighted in purple. A semi-transparent molecular surface for the bound cleavaminium is shown for reference.

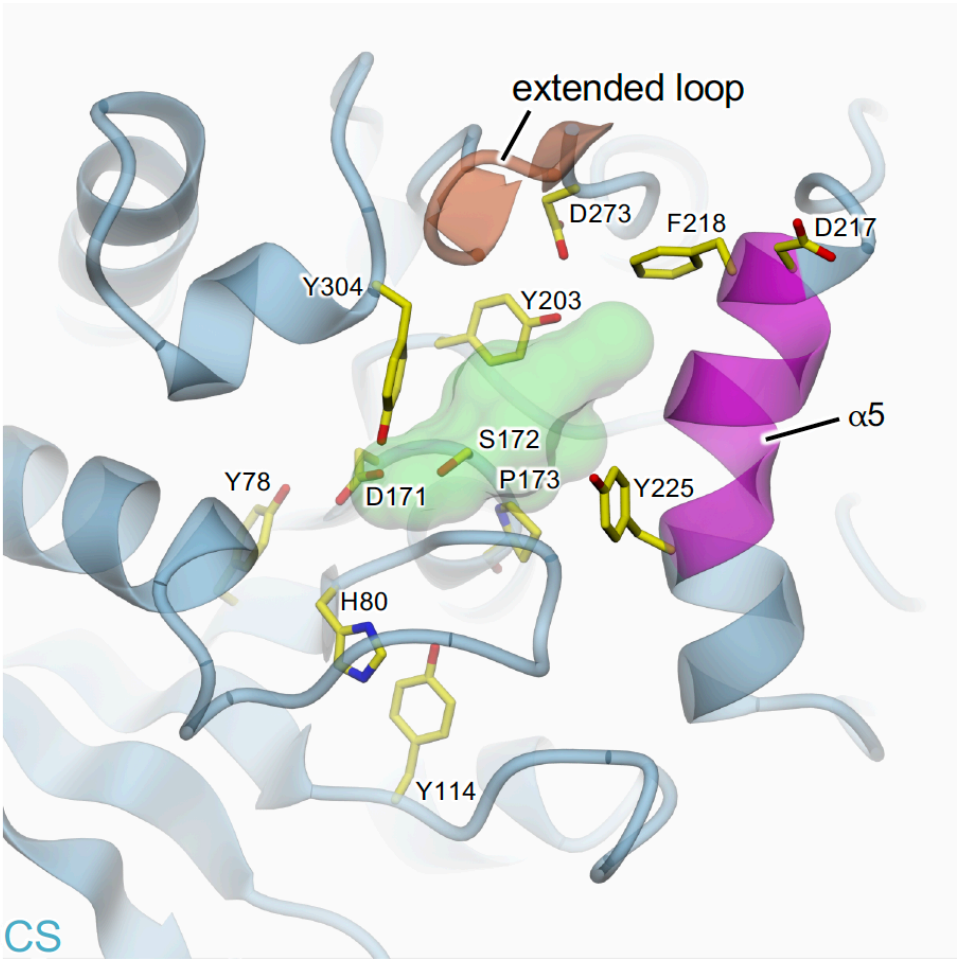

Supplementary Fig. 20. Mutational analysis of CS. **a)** Chromatograms showing the new products made by the mutants with altered product specificity, including (–)-coronaridine iminium **9**, tabersonine **5** and an unknown product (*m/z* 337). (–)-Coronaridine iminium **9** was structurally assigned by successful reduction to (–)-coronaridine **6** by DPAS (see Supplementary Fig. 25). **b)** Activity of all the mutants expressed as percentage of catharanthine **4** produced in 20 min compared to WT enzyme (100 %). Mean value of three distinct replicates ± SD. Each red dot represents a datapoint.

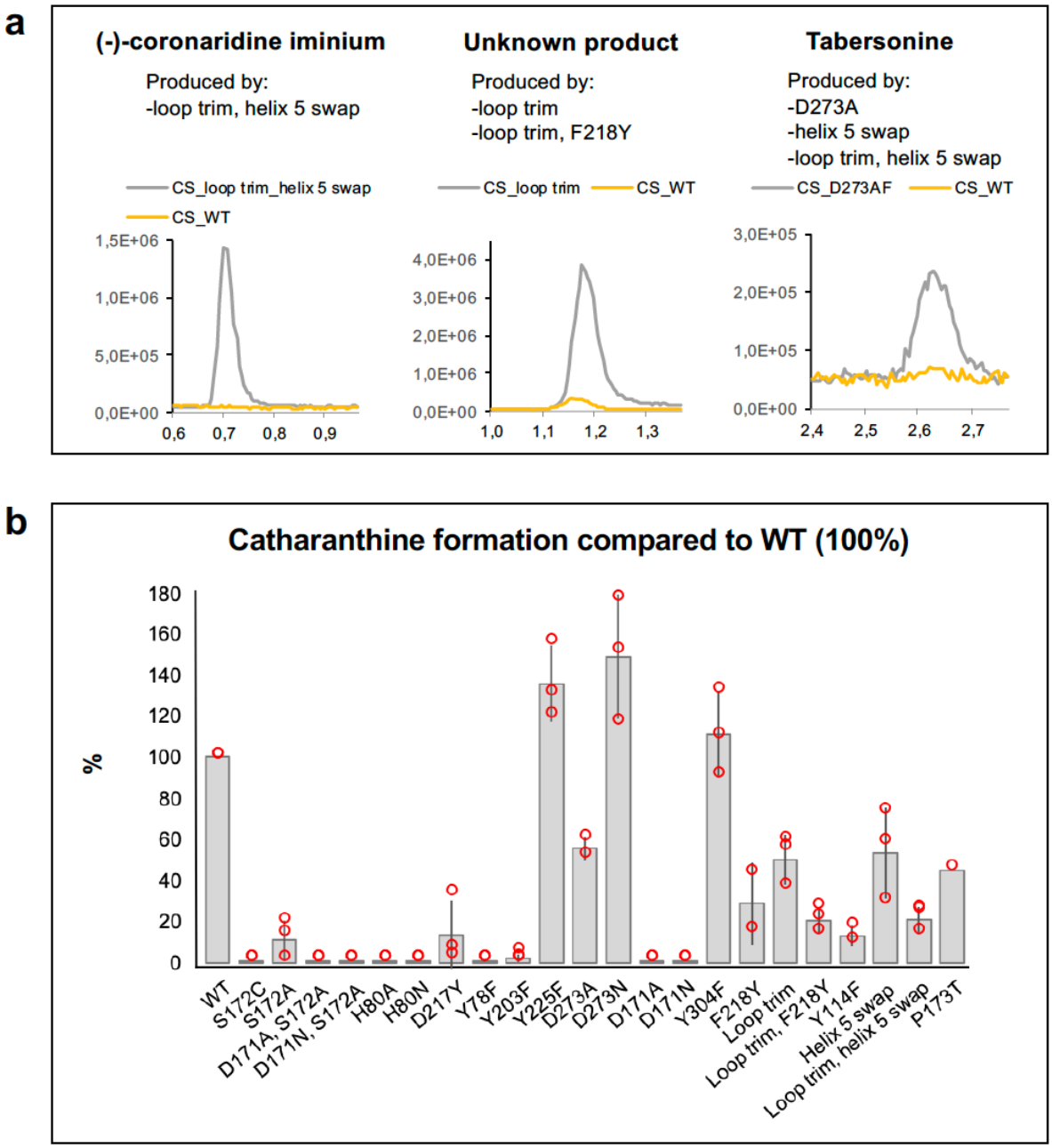

Supplementary Fig. 21. Residues targeted in the mutational analysis of TS. Amino acid residues targeted in this study are shown with yellow carbons. Helix α5 is highlighted in purple. A semi-transparent molecular surface for the docked tabersonine **5** is shown for reference.

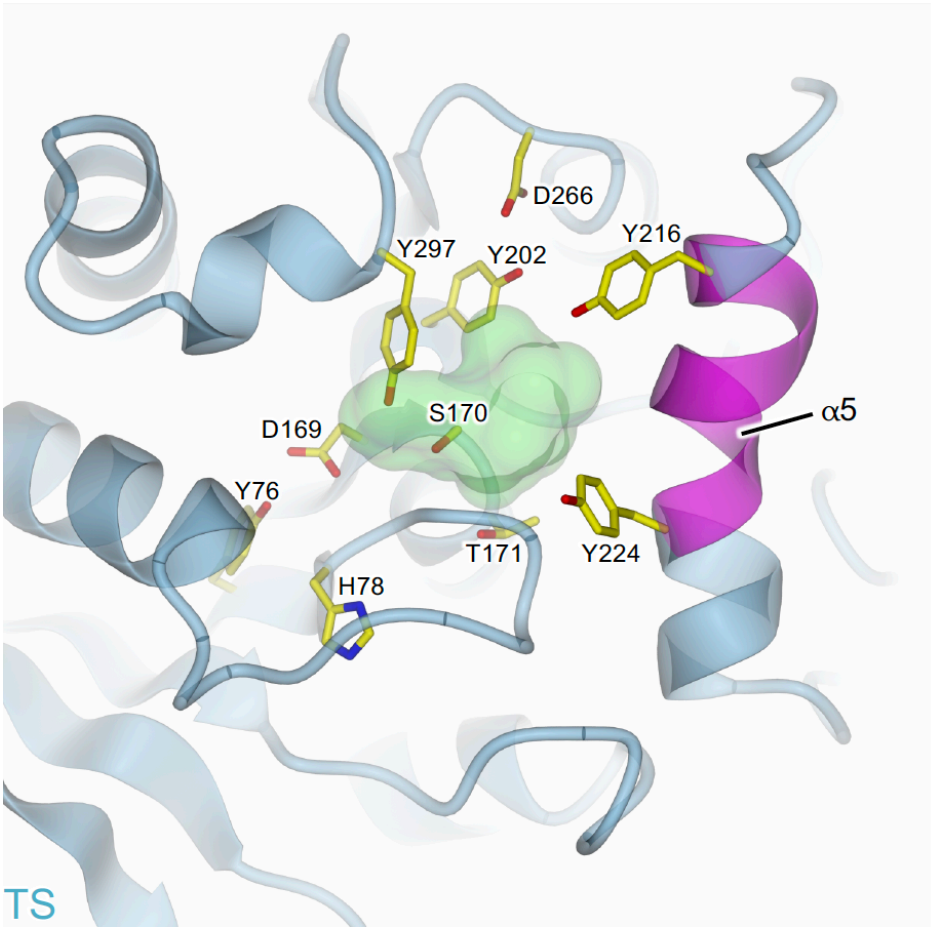

Supplementary Fig. 22. Mutational analysis of TS. **a)** Chromatograms showing the new products made by the mutants with altered product specificity, in this case catharanthine **4** and an unknown product (*m/z* 337). **b)** Activity of all the mutants expressed as percentage of tabersonine **5** produced in 20 min compared to WT enzyme (100 %). Mean of three distinct replicates ± SD. Each red dot represents a datapoint.

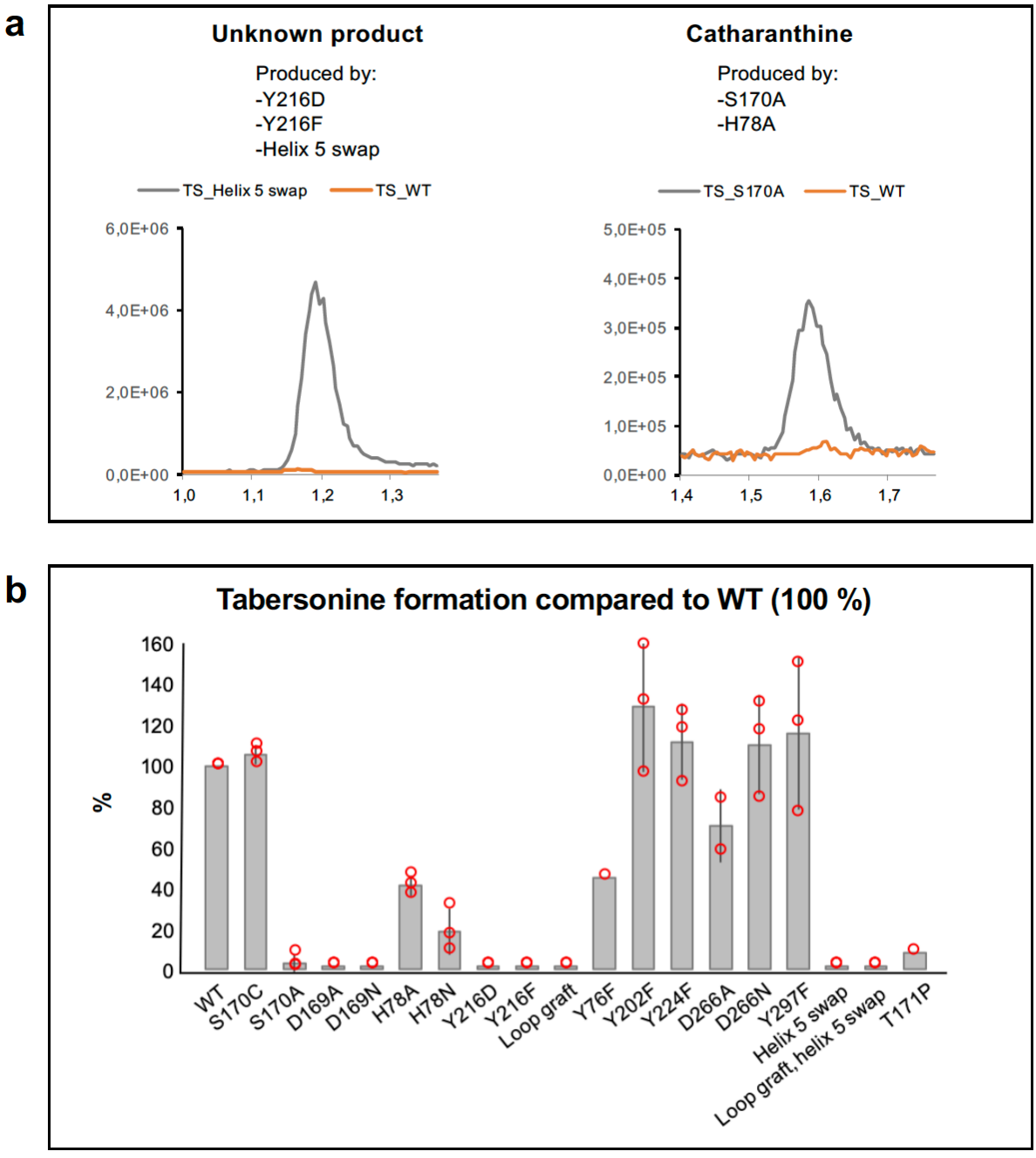

Supplementary Fig. 23. Residues targeted in the mutational analysis of CorS. Amino acid residues targeted in this study are shown with yellow carbons. Helix α5 is highlighted in purple. A semi-transparent molecular surface for the docked coronaridine iminium **9** is shown for reference.

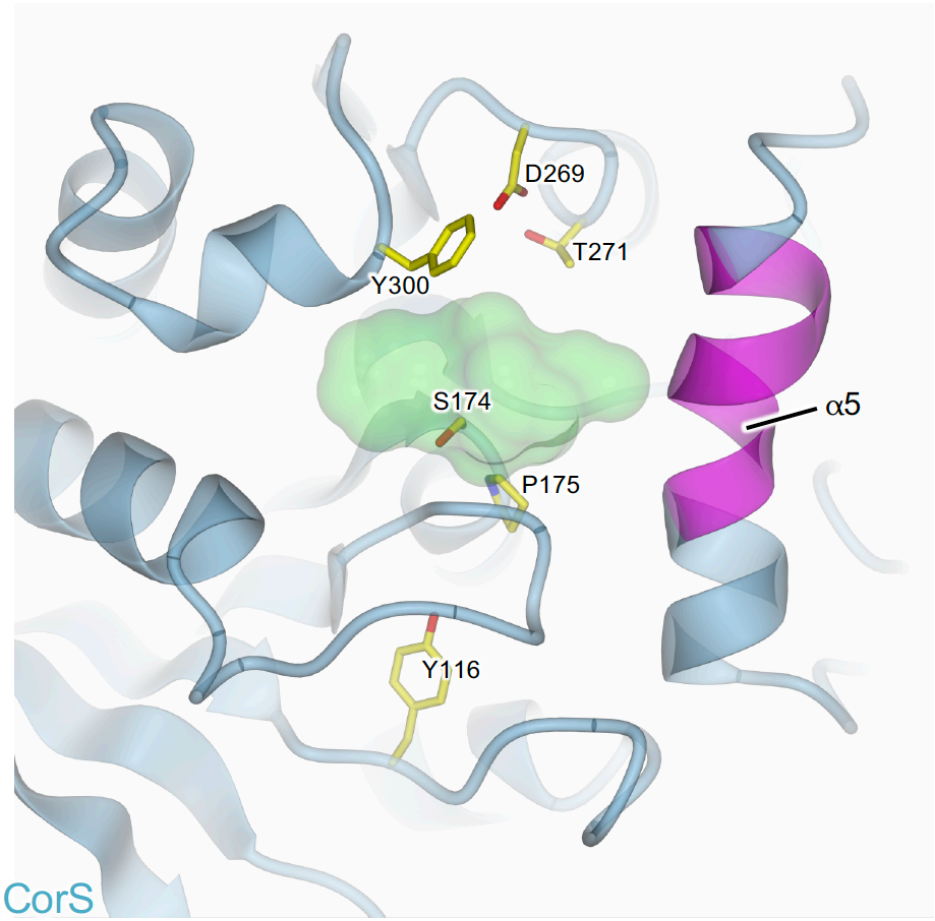

Supplementary Fig. 24. Mutational analysis of CorS. **a)** Chromatograms showing the new products made by the mutants with altered product specificity, in this case catharanthine **4** and tabersonine **5**. **b)** Box and whiskers plot showing the activity of all the mutants expressed as percentage of coronaridine iminium produced in 20 min compared to WT enzyme (100 %). The structure of coronaridine iminium **9** was assigned by the formation of coronaridine upon reduction with DPAS (see Supplementary Fig. 25). Mean of three distinct replicates ± SD. Each red dot represents a datapoint.

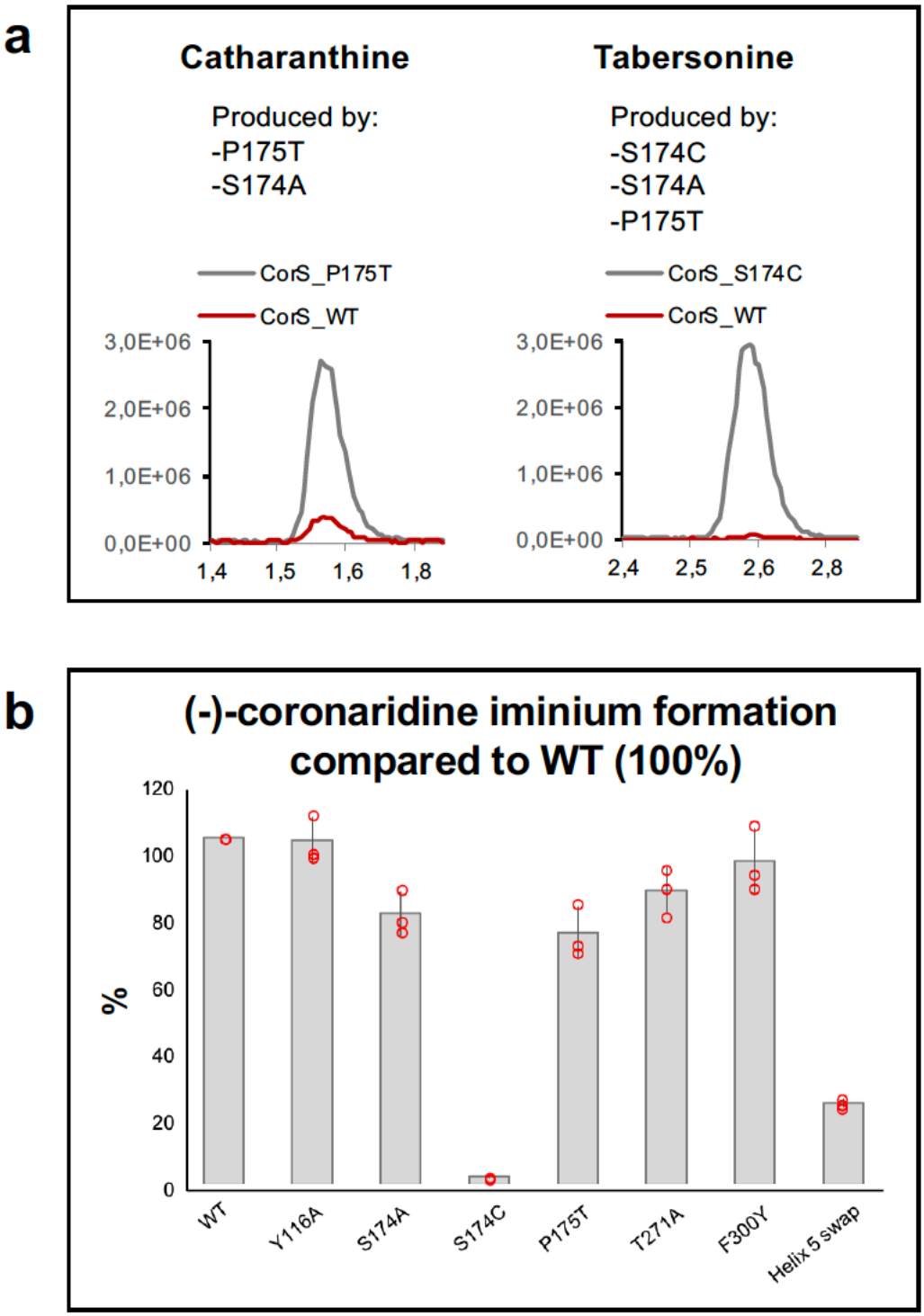

Supplementary Fig. 25. Formation of (–)-coronaridine **6** by a CS mutant. In this mutant, the extended loop was trimmed and the Helix α5 was replaced with the one from TS. Reactions were performed in the presence of TiDPAS, using angryline **3c** as substrate. The stars indicate unknown shunt products (*m/z* 339) formed during the reaction, whilst the peak labeled with V corresponds to the product (–)-vincadifformine.

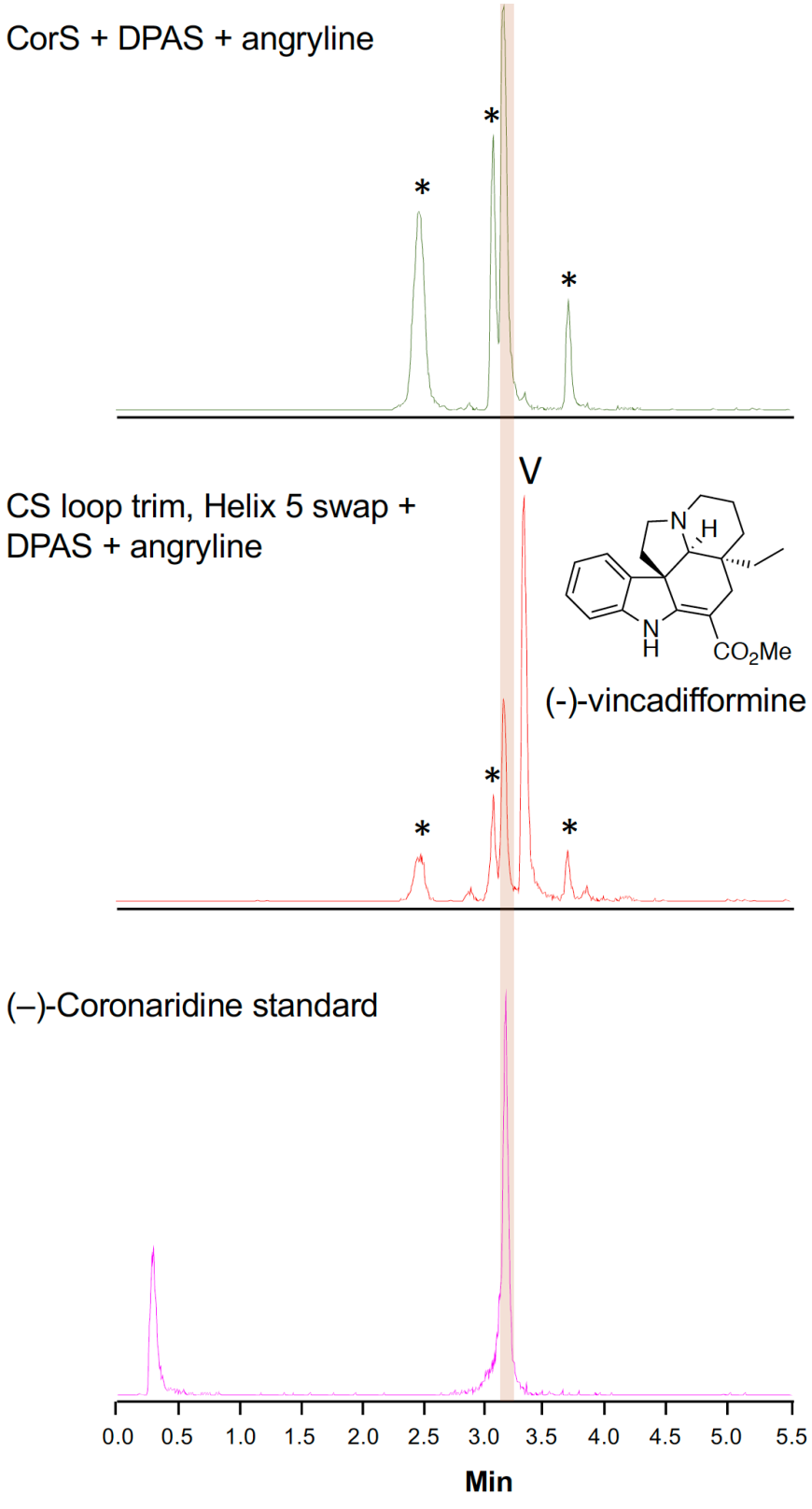

Supplementary Note

Structural Basis of Cycloaddition in Biosynthesis of Iboga and Aspidosperma Alkaloids

Lorenzo Caputi[1#], Jakob Franke[2#], Kate Bussey[3], Scott C. Farrow[3], Ivo Jose Curcino Vieira[4], Clare E. M. Stevenson[3], David M. Lawson*[3], Sarah E. O'Connor*[1]

[1] Max Planck Institute of Chemical Ecology, Department of Natural Product Biosynthesis, Hans-Knöll-Straße 8, 07745 Jena, Germany

[2] Leibniz University Hannover, Centre for Biomolecular Drug Research, Schneiderberg 38, 30167 Hannover, Germany

[3] John Innes Centre, Department of Biological Chemistry, Norwich Research Park, Norwich, NR4 7UH, UK

[4] Laboratorio de Ciencias Quimicas-UENF-Campos dos Goytacazes-RJ, 28013-602, Brazil

[#] These authors contributed equally.

*Correspondence to: oconnor@ice.mpg.de and david.lawson@jic.ac.uk

Production and purification of angryline

Angryline **3c** was produced from stemmadenine acetate (*m/z* 337.19) using sequential reactions of CrPAS and CrDPAS. Initially, 0.25 mg of stemmadenine acetate, 40 μM FAD and 5 μg of CrPAS were combined in a total volume of 500 μL in 50 mM TRIS-HCl buffer pH 8.5 and incubated at 37 °C to form precondylocarpine acetate **2** (*m/z* 395.19). The progress of the reactions was monitored by mass spectrometry. When all the substrate was converted to product (approx. 2h), 1 mg of NADPH and 9 μg of CrDPAS were added to the reaction and incubated for 20 min at 37 °C to obtain angryline (*m/z* 337.19). Multiple reactions were prepared in order to obtain sufficient product for NMR characterization. After completion, the reactions were snap frozen in liquid nitrogen and stored at -80 °C. Angryline **3c** was purified from the other components and some by products present in the reactions, by semi-preparative HPLC on a Dionex ultimate 3000 HPLC system. The reactions were thawed and 500 μL of 90:9:1 MeOH:H_2O:FA were added. The samples were filtered through 0.2 μm PTFE disc filters to remove the precipitated enzymes and injected onto a 250 x 10 mm YMC-Pack Pro C18 column (YMC). Chromatographic separation was performed using 0.1% FA as mobile phase A and acetonitrile as mobile phase B. A linear gradient from 15% B to 45% B was used for purification of the compound followed by a wash at 45% B for 4 min and a re-equilibration step to 15% B for 5 min. Flow rate was 4 mL/min. Elution of angryline was monitored at 330 nm. Fractions containing angryline **3c** were collected, dried under reduced pressure and stored at -80 °C.

NMR data of angryline 3c (CD_3OD, 256 K, 600 MHz).

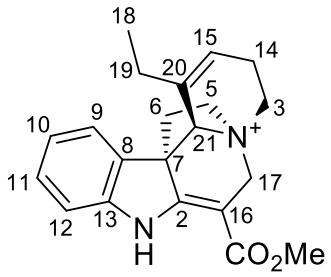

angryline

No	^{13}C	^{1}H (m, *J* in Hz)
2	158.4	-
3	59.5	4.05 (m) 3.76 (m)
5	64.6	4.06 (m) 3.88 (m)
6	40.7	2.66 (m) 2.51 (m)
7	54.5	-
8	128.5	-
9	124.6	7.49 (d, 7.5)
10	123.2	7.06 (dd, 7.6, 7.6)
11	131.2	7.33 (dd, 7.8, 7.8)
12	112.0	7.10 (d, 7.6)
13	146.5	-
14	24.0	2.82 (m) 2.66 (m)
15	121.9	5.66 (s)
16	83.7	-
17	57.1	4.41 (dd, 15.0, 2.0) 4.06 (m)
18	11.7	0.78 (t, 7.3)
19	25.6	1.43 (m)
20	134.3	-
21	69.8	5.11 (s)
COOMe	166.6	-
COOMe	51.9	3.78 (s)

NMR spectra for angryline 3c (CD_3OD, 256 K, 600 MHz). ^{1}H (16 scans), ^{13}C (160 scans), COSY (10 scans), NOESY (70 scans), HSQC (40 scans) and HMBC (160 scans).

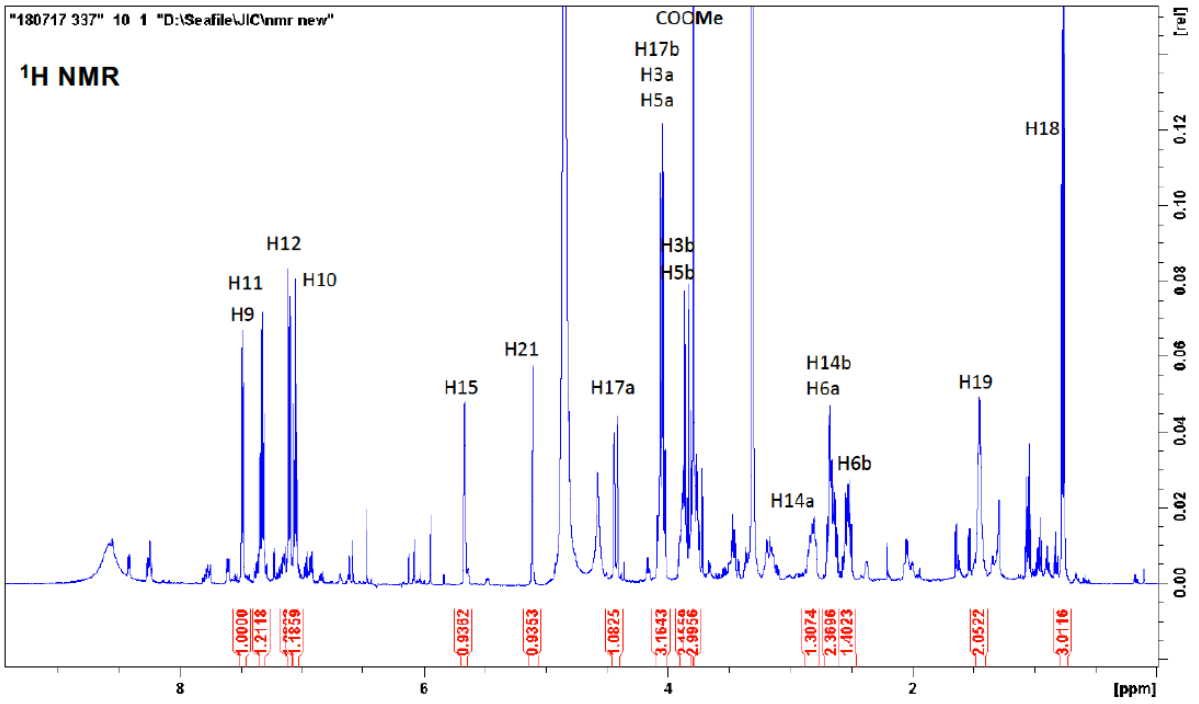

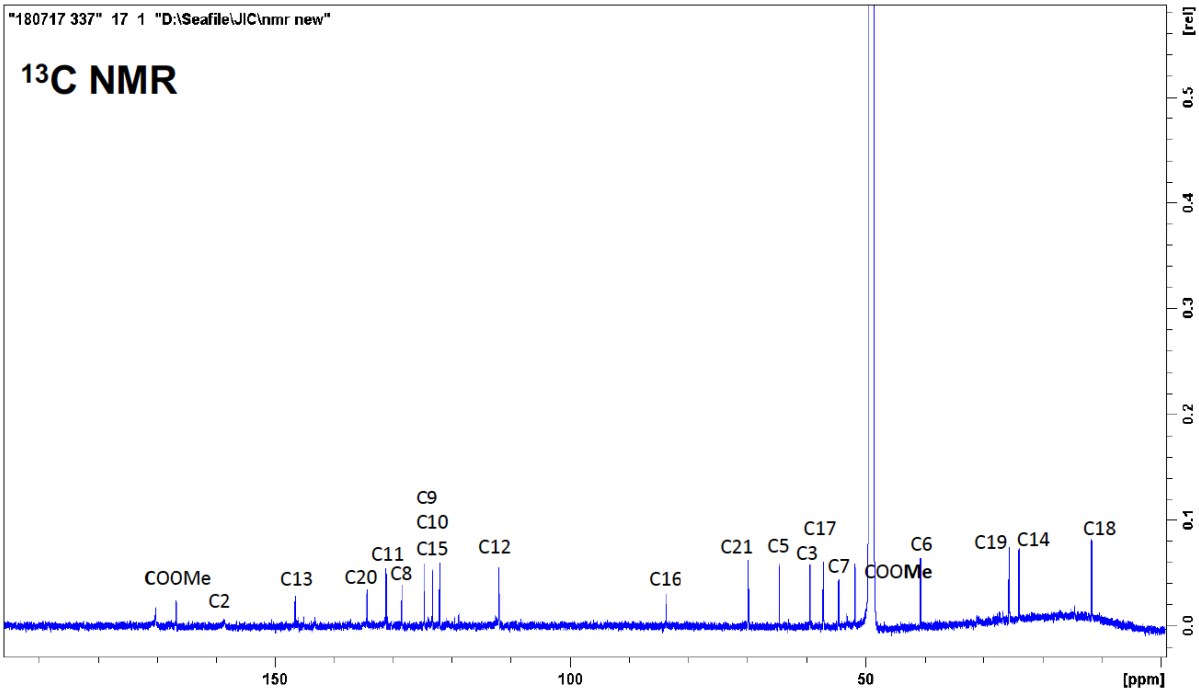

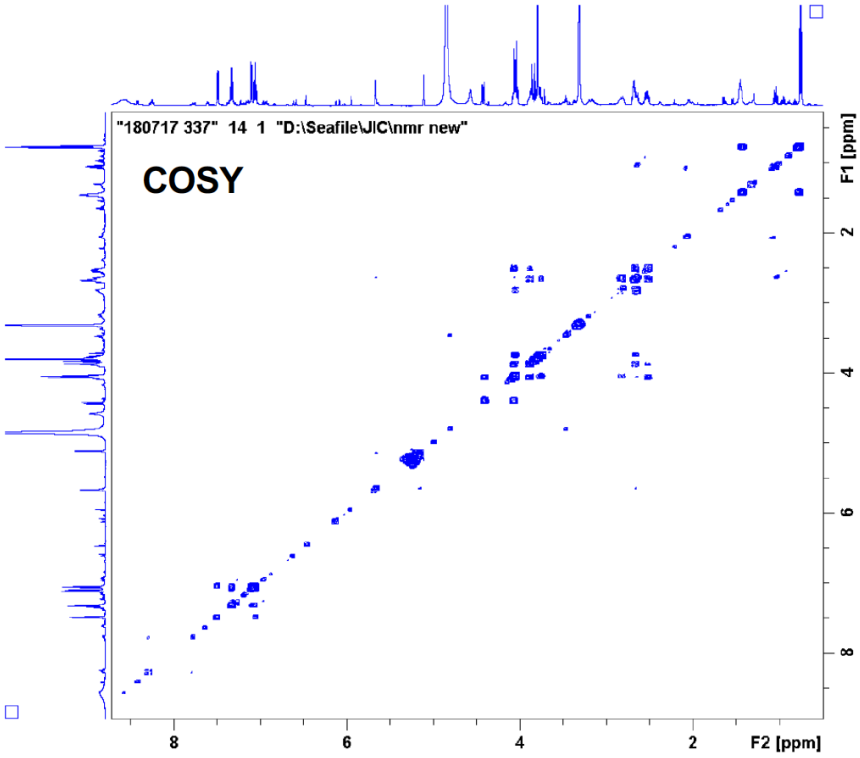
"180717 337" 14 1 "D:\Seafile\JIC\nmr new"
COSY
F1 [ppm]
F2 [ppm]
8
6
4
2

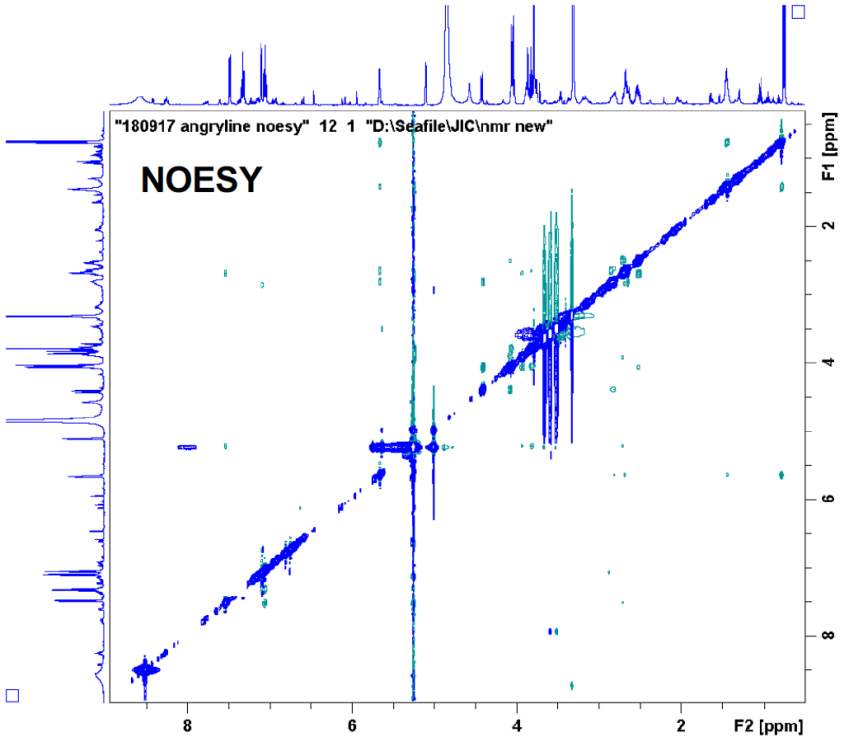
"180917 angryline noesy" 12 1 "D:\Seafile\JIC\nmr new"
NOESY
F1 [ppm]
F2 [ppm]
8
6
4
2

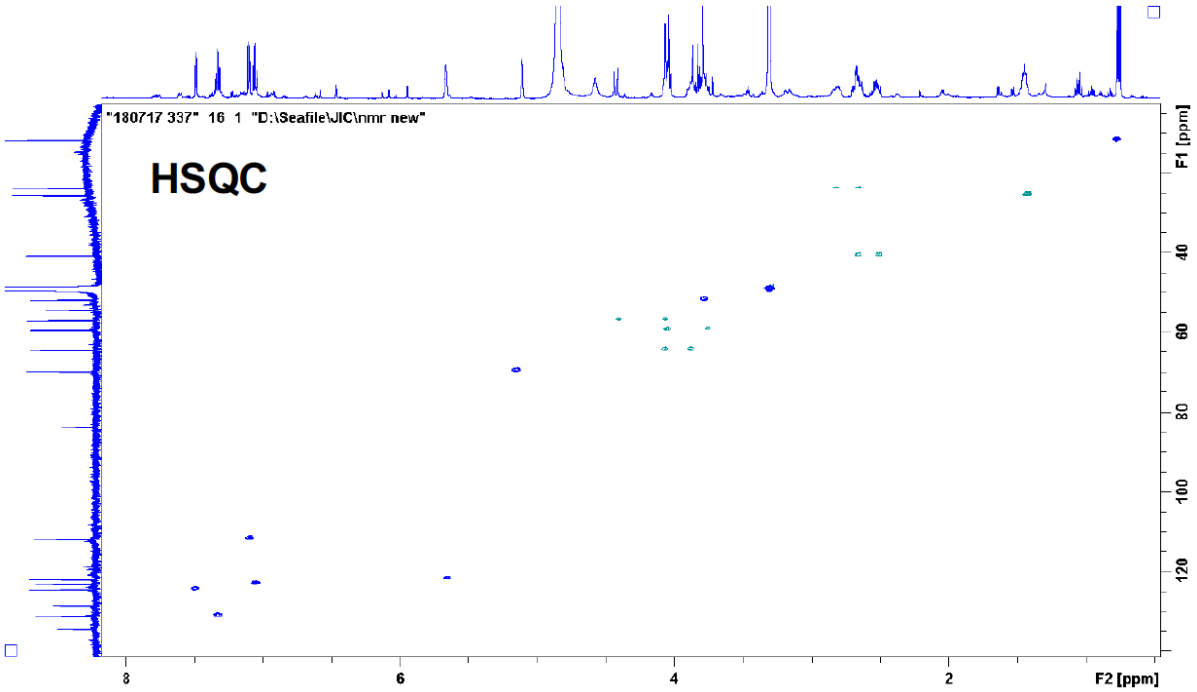
"180717 337" 16 1 "D:\Seafile\JIC\nmr new"
HSQC
F1 [ppm]
40
60
80
100
120
8
6
4
2
F2 [ppm]

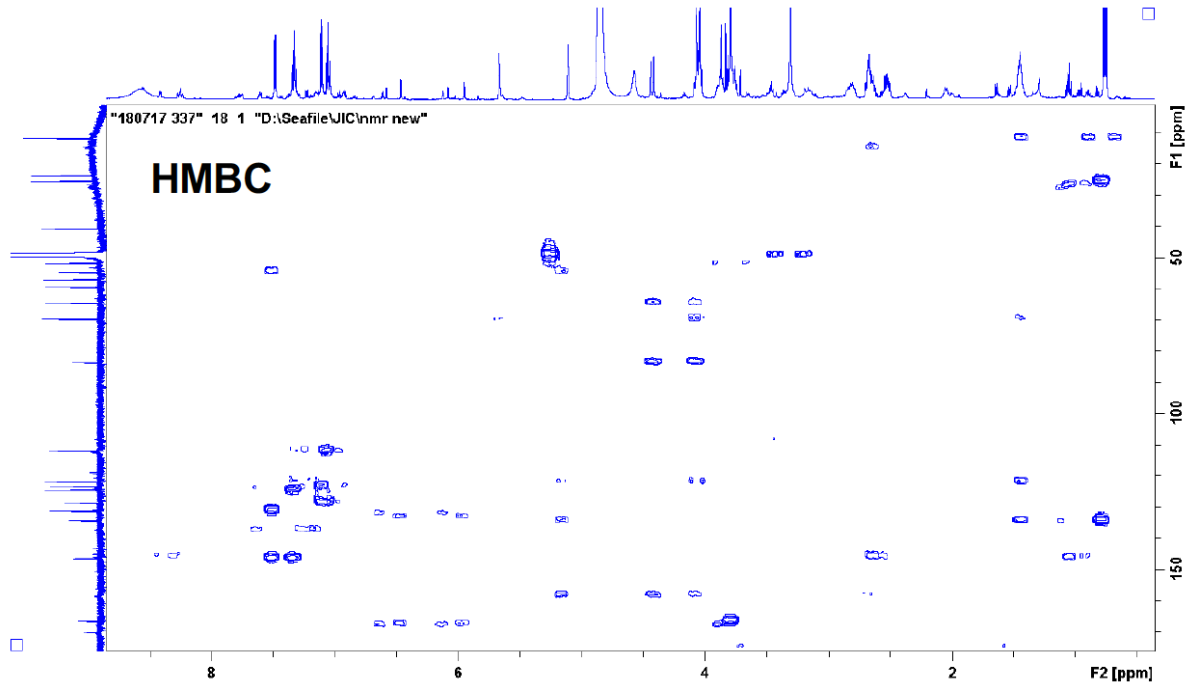
"180717 337" 18 1 "D:\Seafile\JIC\nmr new"
HMBC
F1 [ppm]
50
100
150
8
6
4
2
F2 [ppm]

Key NMR correlations (COSY, HMBC and NOESY) of angryline **3c**.

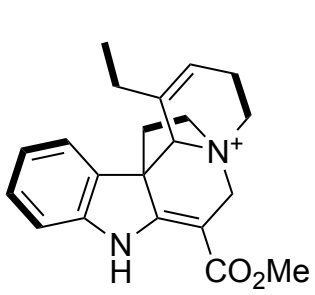

COSY

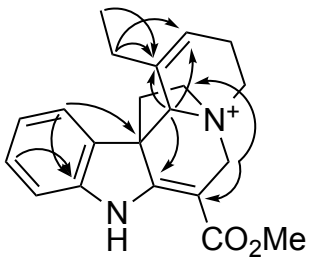

HMBC

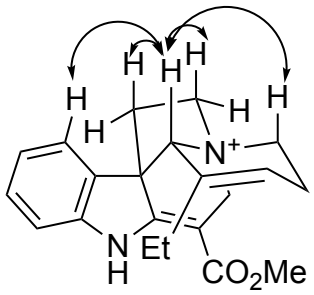

NOESY

Comparison of NMR shifts of angryline **3c** with related monoterpene indole alkaloids supporting the presence of a quaternary nitrogen atom.

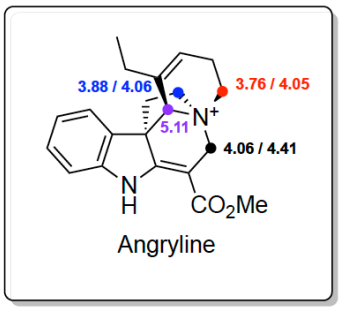

Angryline

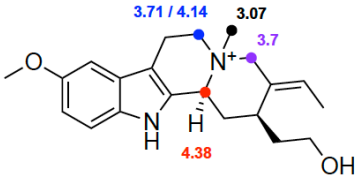

10-Methoxy-4-methylgeissoschizol

Taveira, J.J. *et al. Phytochemistry* **31**, 2507-2511 (1992)

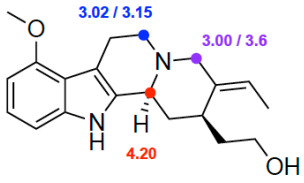

9-Methoxygeissoschizol

Mavar-Manga, H. *et al. Phytochemistry* **43**, 1125-1127 (1996)

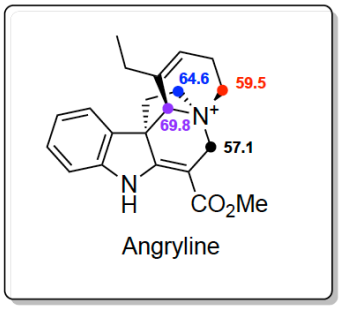

Angryline

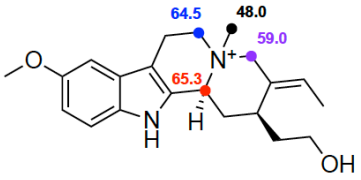

10-Methoxy-4-methylgeissoschizol

Taveira, J.J. *et al. Phytochemistry* **31**, 2507-2511 (1992)

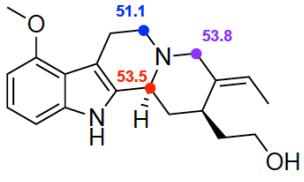

9-Methoxygeissoschizol

Mavar-Manga, H. *et al. Phytochemistry* **43**, 1125-1127 (1996)

Comparison of NMR shifts of angryline **3c** with related monoterpene indole alkaloids supporting the presence of a C2-C16 double bond.

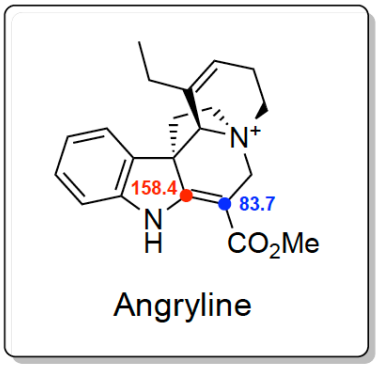

Angryline

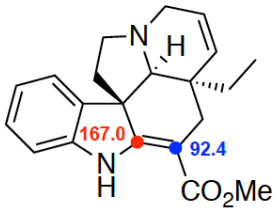

Tabersonine

Zang, Y. *et al. Molecules* **24**, 1256 (2019)

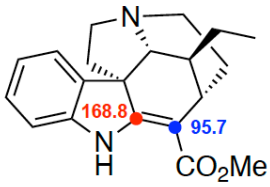

Tubotaiwine

Yamauchi, T. *et al. Phytochemistry* **29**, 3321-3325 (2019)